

**OFFICE  
OF  
RESEARCH**

**LEHIGH UNIVERSITY**



**AD743201**

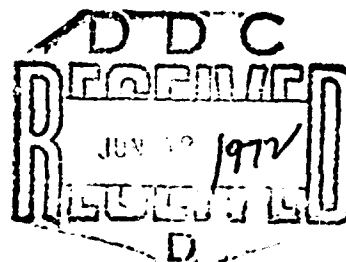
Themis Project: Fluid Amplifiers  
Office of Naval Research, Code 461  
Contract No. N00014-69-A-0417

Technical Report No. 8

**DYNAMIC MODELING OF THE  
BISTABLE FLUID AMPLIFIER**

by  
James F. Ries

January 1972



Department of Mechanical Engineering  
and Mechanics  
Lehigh University  
Bethlehem, Pennsylvania

Reproduced by  
NATIONAL TECHNICAL  
INFORMATION SERVICE  
Springfield, Va. 22151

15 R

ACCESSION FOR	
DATA	WHITE SECTION <input checked="" type="checkbox"/>
NOG	BUFF SECTION <input type="checkbox"/>
MAN. CEO.	<input type="checkbox"/>
JUSTIFICATION	
BY	
DISTRIBUTION/AVAILABILITY CODES	
DIST.	AVAIL. AND OF SPECIAL
<b>A</b>	

Distribution of this document is unlimited.

Reproduction in whole or in part is permitted for any purpose of the United States Government.

Unclassified

Security Classification

## DOCUMENT CONTROL DATA - R &amp; D

Security classification of title, body of abstract and indexing annotation must be entered when the overall report is classified

1. ORIGINATING ACTIVITY (Corporate author)		2a. REPORT SECURITY CLASSIFICATION	
Lehigh University - Bethlehem, Pa. 18015 Department of Mechanical Engineering and Mechanics		Unclassified	
3. REPORT TITLE		2b. GROUP	
DYNAMIC MODELING OF THE BISTABLE FLUID AMPLIFIER			
4. DESCRIPTIVE NOTES (Type of report and inclusive dates)			
Technical Report			
5. AUTHOR(S) (First name, middle initial, last name)			
James P. Ries			
6. REPORT DATE	7a. TOTAL NO. OF PAGES	7b. NO. OF REFS	
January 1972	66	24	
8a. CONTRACT OR GRANT NO.	9a. ORIGINATOR'S REPORT NUMBER(S)		
N00014-69-A-0417	No. 8		
b. PROJECT NO.	9b. OTHER REPORT NO(S) (Any other numbers that may be assigned this report)		
c.			
d.			
10. DISTRIBUTION STATEMENT			
Distribution of this report is unlimited.			
11. SUPPLEMENTARY NOTES		12. SPONSORING MILITARY ACTIVITY	
13. ABSTRACT			
<p>An analytical model for the dynamic response of a bistable fluid amplifier with straight walls is presented. The model represents the dynamic changes which take place in an amplifier during the early phases of switching. The state of the amplifier at any instant of time is identified by a set of system equations whose input function is the mass flow rate from the control port. The system variables, constants and equations are arranged in nondimensional form in order to organize and facilitate the solution.</p> <p>In the second half of the report, the system equations are used to prepare an analog simulation of the amplifier. The coupling between system variables and the feedback mechanisms present in the model can be easily identified from this simulation.</p> <p>Computer results were obtained for this simulation for a number of input conditions and amplifier geometries. One of the more interesting results of this study is the dynamic change of pressure within the separation region (bubble). With a sudden increase in control flow, the bubble undergoes an initial decrease in pressure followed by its expected rise to a new equilibrium condition. Because of this result, the jet attachment point moves toward the power nozzle for a short duration of time.</p>			

DD FORM 1473

1 NOV 65

(PAGE 1)

Unclassified

Security Classification

S/N 0101-807-6801

Unclassified

Security Classification

14	KEY WORDS	LINK A		LINK B		LINK C	
		ROLE	WT	ROLE	WT	ROLE	WT
	bistable attachment dynamic response						

Unclassified

Security Classification

Themis Project: Fluid Amplifiers  
Office of Naval Research, Code 461  
Contract No. N00014-69-A-0417

Technical Report No. 8

DYNAMIC MODELING OF THE  
BISTABLE FLUID AMPLIFIER

by  
James P. Ries



January 1972

Department of Mechanical Engineering and Mechanics  
Lehigh University  
Bethlehem, Pennsylvania

Distribution of this document is unlimited.  
Reproduction in whole or in part is permitted for any purpose of  
the United States Government.

## ABSTRACT

An analytical model for the dynamic response of a bistable fluid amplifier with straight walls is presented. The model represents the dynamic changes which take place in an amplifier during the early phases of switching. The state of the amplifier at any instant of time is identified by a set of system equations whose input function is the mass flow rate from the control port. The system variables, constants and equations are arranged in nondimensional form in order to organize and facilitate the solution.

In the second half of the report, the system equations are used to prepare an analog simulation of the amplifier. The coupling between system variables and the feedback mechanisms present in the model can be easily identified from this simulation.

Computer results were obtained for this simulation for a number of input conditions and amplifier geometries. One of the more interesting results of this study is the dynamic change of pressure within the separation region (bubble). With a sudden increase in control flow, the bubble undergoes an initial decrease in pressure followed by its expected rise to a new equilibrium condition. Because of this result, the jet attachment point moves toward the power nozzle for a short duration of time.

## TABLE OF CONTENTS

	page
ABSTRACT	ii
TABLE OF CONTENTS	iii
LIST OF FIGURES	iv
NOMENCLATURE	vi
I. INTRODUCTION	1
II. MODELING THE DYNAMIC RESPONSE	3
A. Amplifier Description	3
B. Geometric Relations	4
C. Fluid Relations	5
III. NONDIMENSIONAL MODEL	8
IV. ANALOG MODEL AND SIMULATION	12
A. Steady State Response Simulation	13
B. Dynamic Response Simulation	13
V. RESULTS	15
VI. CONCLUSIONS	17
APPENDIX	19
ACKNOWLEDGEMENT	28
REFERENCES	29
FIGURES	

## LIST OF FIGURES

- Figure 1. Geometry of the Bistable Amplifier.
- Figure 2. Geometry of the Attached Jet.
- Figure 3. Block Diagram for the Amplifier in Physical Variables.
- Figure 4. Analog Diagram for the Amplifier in Nondimensional System Variables.
- Figure 5. Steady State Results for the Entrainment and Recirculating Mass Flows ( $X_1$ ,  $X_2$ ).
- Figure 6. Steady State Results for the Bubble Mass ( $X_4$ ).
- Figure 7. Steady State Results for the Bubble Pressure ( $X_5$ ).
- Figure 8. Steady State Results for the Reattachment Length ( $X_6$ ).
- Figure 9. Steady State Results for Jet Radius of Curvature ( $X_7$ ).
- Figure 10. Steady State Results for Reattachment Radius ( $X_8$ ).
- Figure 11. Steady State Results for Bubble Volume ( $X_9$ ).
- Figure 12. Steady State Results for Angle  $\beta$  ( $X_{10}$ ).
- Figure 13. Steady State Results for Angle  $\theta$  ( $X_{11}$ ).
- Figure 14. Steady State Results for Angle  $\phi$  ( $X_{12}$ ).
- Figure 15. Dynamic Input for Case A - Small Change in Control Flow ( $X_3$ ).
- Figure 16. Dynamic Response of Entrainment and Recirculating Flows ( $X_1$ ,  $X_2$ ) for Case A.
- Figure 17. Dynamic Response of Bubble Mass ( $X_4$ ) for Case A.
- Figure 18. Dynamic Response of Bubble Pressure ( $X_5$ ) for Case A.
- Figure 19. Dynamic Response of Reattachment Length ( $X_6$ ) for Case A.
- Figure 20. Dynamic Response of Jet Radius of Curvature ( $X_7$ ) for Case A.



- Figure 21. Dynamic Response of Reattachment Radius ( $X_8$ ) for Case A.
- Figure 22. Dynamic Response of Bubble Volume ( $X_9$ ) for Case A.
- Figure 23. Dynamic Response of Angle  $\beta$  ( $X_{10}$ ) for Case A.
- Figure 24. Dynamic Response of Angle  $\theta$  ( $X_{11}$ ) for Case A.
- Figure 25. Dynamic Response of Angle  $\phi$  ( $X_{12}$ ) for Case A.
- Figure 26. Dynamic Input for Case B - Large Change in Control Flow ( $X_3$ ).
- Figure 27. Dynamic Response of Entrainment and Recirculating Flows ( $X_1, X_2$ ) for Case B.
- Figure 28. Dynamic Response of Bubble Mass ( $X_4$ ) for Case B.
- Figure 29. Dynamic Response of Bubble Pressure ( $X_5$ ) for Case B.
- Figure 30. Dynamic Response of Reattachment Length ( $X_6$ ) for Case B.
- Figure 31. Dynamic Response of Jet Radius of Curvature ( $X_7$ ) for Case B.
- Figure 32. Dynamic Response of Reattachment Radius ( $X_8$ ) for Case B.
- Figure 33. Dynamic Response of Bubble Volume ( $X_9$ ) for Case B.
- Figure 34. Dynamic Response of Angle  $\beta$  ( $X_{10}$ ) for Case B.
- Figure 35. Dynamic Response of Angle  $\theta$  ( $X_{11}$ ) for Case B.
- Figure 36. Dynamic Response of Angle  $\phi$  ( $X_{12}$ ) for Case B.

## NOMENCLATURE

$b$	power nozzle width
$C$	control port width
$d$	amplifier thickness
$D$	setback of the amplifier wall from the power nozzle
$K_i$	nondimensional system constants
$\dot{m}_c$	control mass flow rate
$\dot{m}_e$	entrainment mass flow rate
$\dot{m}_r$	recirculated mass flow rate
$\dot{M}$	mass flow rate from power nozzle
$M_B$	separation bubble mass
$P_\infty$	pressure outside the bubble
$P_B$	separation bubble pressure
$r$	radius to the attachment point
$R$	radius of the attached jet centerline
$R_a$	gas constant for air
$t$	real time
$T$	air temperature inside the bubble
$V_B$	separation bubble volume
$X_i$	nondimensional system variables
$X_o$	distance to origin of power jet
$X_r$	distance along the wall to the attachment point
$X_v$	distance to the vent

$\alpha$	amplifier wall angle
$\beta$	angle of the power jet at the nozzle exit
$\Gamma$	sum of four angles
$\theta$	attachment angle of the power jet
$\eta$	attaching streamline parameter
$\sigma$	Goertler spread parameter
$\phi$	small angle
$\rho$	power jet density
$T$	nondimensional time

## I. INTRODUCTION

Many control systems which are in use today depend on an assortment of pneumatic and hydraulic devices. These components utilize the characteristics of flowing fluids for actuation, decision making and amplification. The major class of such devices have moving parts and depend on the interaction between mechanical and fluidic systems. Some common amplifiers with moving parts are:

1. spool valves
2. flapper valves
3. ball valves
4. diaphragm valves

During the past twelve years a second class of fluid amplifiers has been developed. These devices have no moving parts and are referred to as pure fluid amplifiers. Their input is a fluidic signal which produces an amplified change in the output fluid flow. The geometry of the amplifier remains fixed during its operation. These pure fluid amplifiers can be further subdivided into two categories. Those having a continuous input-output relationship are called analog or proportional amplifiers. The second group have digital characteristics and are known as bistable or two-state amplifiers.

This second class of pure fluid amplifiers have one or more stable output states and are used in the design of logic systems. Several of these fluid logic devices are connected to achieve different logic or switching functions. Four of the more common elements are:

1. Induction amplifier
2. Turbulence amplifier
3. Focused jet amplifier
4. Wall-attachment amplifier

Modeling of the fourth element, the wall-attachment amplifier, is the subject of this report.

The development of the wall-attachment amplifier was first announced at Diamond Ordnance Fuze Laboratories (now Harry Diamond Laboratories, HDL) in 1960. Operation of this amplifier depends on the Coanda

effect which is the natural attachment of a free jet to an adjacent wall. A low pressure region or bubble exists between the wall, the jet and the point of attachment. The pressure difference across the jet establishes the curvature of the jet as it exits from the output duct on the attached side. The addition of control flow into the low pressure region causes the bubble to grow. This growth results in the jet attaching to the opposite wall and issuing from the output duct on that side. This process takes place in a few milliseconds and establishes the bistable relationship for the amplifier.

Initial studies on the reattachment of free jets to inclined and offset walls were done by many different investigators. The work of Bourque and Newman [1] has served as the basis for much of the recent studies [2, 3, 4]. The application of this work to the amplifier resulted in studies on steady state performance and the effects of amplifier geometry on attachment. The works of Sher [5] and Levin and Manion [6] are indicative of these types of studies [7, 8, 9].

The next phase of research dealt with the switching process and its characteristics. A number of papers have been written on the subject [10, 11, 12, 13, 14]. Kirshner [15] defined the three types of switching (1) terminated wall (2) contacting-both-walls and (3) splitter switching, while Müller [11] described a critical attachment angle type of switching.

Most recent studies have concentrated on the dynamic modeling of the switching process itself. Savkar, Hansen and Keller [14] reported some experimental values for switching times while Lush [16, 17] compared experimental values of switching times with a theoretical prediction. Recently theoretical and experimental results for the contacting-both-walls type of switching have been obtained by Özgü and Stenning [22]. Although many investigators [18, 19, 20, 21] have contributed to the study, a complete description of the switching process has not been obtained. This project was undertaken in an attempt to provide some understanding of the early phases of dynamic switching in the wall-attachment amplifier.

## II. MODELING THE DYNAMIC RESPONSE

### A. Amplifier Description

The bistable amplifier to be analyzed is the standard, sloping, straight wall type. The control port is perpendicular to the power jet inlet and has width  $C$ . The geometry of this particular amplifier is shown in Figure 1. The amplifier is also considered to be symmetric about its centerline with the parameters  $D$ ,  $\alpha$  and  $X_v$  defining the offset, wall angle and distance to the vents.

In an equilibrium state the jet is attached to one wall of the amplifier in such a manner as to form a region of uniform pressure called the separation bubble. This bubble region maintains a constant volume and mass as long as the net mass flow into the region is zero. The centerline of the jet is assumed to be a circular arc of radius  $R$  which leaves the center of the power jet at an angle  $\beta$ . This arc intersects the amplifier wall at an angle  $\theta$  and at a point determined by the geometry.

Outer boundary of the separation bubble is formed by the attaching streamline of the fluid jet profile. This arc is given by the distance  $y$  from the circular arc measured along a radius vector. The remaining boundary of the bubble is formed by the fixed boundary of the amplifier. The jet attaches to the wall at a point defined by  $X_r$ . Geometry of the amplifier along with the attached jet is shown in Figure 2.

Before an analytical model can be developed several assumptions must be made concerning the jet behavior and the other interactions within the amplifier.

1. The attached jet has a centerline which follows a circular arc of radius  $R$ .
2. The attached jet is turbulent and has a Goertler velocity profile.
3. The thickness of the two dimensional jet is  $d$ .
4. Pressure inside the separation bubble is uniform throughout the region.

5. The width of the jet is small compared to the radius.
6. Momentum interaction between the control and power jet occurs at a discrete point.
7. The fluid within the separation region behaves as an ideal gas.

From these assumptions and the geometry of the amplifier a dynamic model of the amplifier can be developed. This model which represents the state of the amplifier at any instant of time will be represented by a set of system variables. These variables are related by a set of algebraic and differential equations referred to as system equations.

#### B. Geometric Relations

A number of system equations can be determined from the geometry of the amplifier shown in Figure 2. By equating distances perpendicular to the wall of the amplifier the following equation results.

$$R \cos (\alpha + \beta) = r \cos \theta + (D + \frac{b}{2} - C \tan \alpha) \cos \alpha \quad (1)$$

At the attachment point the length  $r$  can be written,

$$r = R - \left(\frac{\eta}{\sigma}\right) R(\beta + \alpha + \theta) - \eta \left(\frac{X_o}{b}\right) \quad (2)$$

where  $\eta$  defines the attaching streamline,  $\sigma$  is the Goertler spread parameter and  $X_o$  determines the virtual origin of the jet. The small angle  $\phi$  can be determined from the other dimensions.

$$\sin \phi = \frac{(b/2) \sin \beta}{(1 - bR \cos \beta + b^2/4)^{1/2}} \quad (3)$$

By introducing a new variable  $\Gamma$  ,

$$\Gamma = \phi + \beta + \alpha + \theta \quad (4)$$

the expression for the bubble volume ( $V_B$ ) can be simplified. The development of the following equation is given in Appendix A.

$$\begin{aligned} V_B = & d \left\{ \frac{1}{2} \left( R - \frac{b}{2} \cos (\beta + \phi) \right)^2 \Gamma - \left( R - \frac{b}{2} \cos (\beta + \phi) \right) \frac{\eta}{\sigma} R \frac{\Gamma^2}{2} \right. \\ & + \left( \eta \frac{R}{\sigma} \right)^2 \frac{\Gamma^3}{6} - \frac{1}{2} r^2 \cos^2 \theta [\tan (\beta + \phi + \alpha) + \tan \theta] \\ & \left. + \frac{1}{2} [D - C \tan \alpha]^2 \left[ \frac{\sin(\beta + \phi) \sin(90 + \alpha)}{\sin(90 - \alpha - \beta - \phi)} \right] \right\} \quad (5) \end{aligned}$$

Finally, the point of reattachment,  $X_r$ , can be calculated.

$$X_r = [R \sin \beta - C] / \cos \alpha + (r \cos \theta) \tan \alpha + r \sin \theta \quad (6)$$

### C. Fluid Relations

Additional equations can be obtained by considering the conditions of the fluid within the bubble region. Assuming that the entrapped fluid behaves as an ideal gas with uniform pressure  $P_B$ , volume  $V_B$  and mass  $M_B$  the following

$$P_B V_B = M_B R_a T \quad (7)$$



represents the equation of state where  $R_a$  (gas constant) and  $T$  (temperature) remain constant. Mass is being added to the region from the control port at the rate  $\dot{m}_c$ . The power jet entrains mass from the region at a rate  $\dot{m}_e$  and recirculates mass at a rate  $\dot{m}_r$ . The change of mass inside the bubble can be expressed as,

$$\frac{dM_B}{dt} = \dot{m}_c + \dot{m}_r - \dot{m}_e \quad (8)$$

The angle  $\beta$  can be determined by considering the momentum interaction between the control and power jets,

$$\tan \beta = \frac{\dot{m}_c^2 b}{\dot{M}_C^2} \quad (9)$$

where  $\dot{M}$  is the mass flow rate of the power jet.

The motion of the power jet is represented by a term which depends on the rate of change of radius  $R$  in the following curvature equation.

$$\frac{3\dot{M}}{bd\sigma} \sqrt{\frac{x_o}{R\Gamma}} \frac{dR}{dt} - \frac{\dot{M}^2/\rho}{R} bd^2 = P_B - P_\infty \quad (10)$$

Development of this equation along with a discussion of the additional term is given in Appendix B. Parameter  $\rho$  is the density of the power jet and is assumed to remain constant.

Using the Goertler profile for the velocity distribution of the jet, the entrainment and recirculation flow rates can be determined. See Appendix C.

$$\dot{m}_r = \dot{M} \left\{ \frac{3R}{4b\sigma} (\beta + \alpha + \theta) + \frac{1}{4} \right\}^{1/2} (1 - \tanh \eta) \quad (11)$$

$$\dot{m}_e = \dot{M} \left[ \left\{ \frac{3R}{4b\sigma} (\beta + \alpha + \theta) + \frac{1}{4} \right\}^{1/2} - 0.5 \right] \quad (12)$$

The model, at this point, describes the dynamic growth(collapsing) of the separation region (bubble) due to changes in control mass flow  $\dot{m}_c$ . With  $\dot{m}_c$  as the input, the state of the amplifier at any instant of time is described by thirteen variables listed in the table below.

Table 1

Notation	Description
1. $\dot{m}_e$	entrained mass flow rate
2. $\dot{m}_r$	recirculated mass flow rate
3. $\dot{m}_c$	control mass flow rate (input)
4. $M_B$	bubble mass
5. $P_B$	bubble pressure
6. $X_r$	reattachment length
7. $R$	radius of curvature of jet
8. $r$	radius to reattachment point
9. $V_B$	bubble volume
10. $\beta$	initial jet deflection angle
11. $\theta$	angle of attachment
12. $\phi$	small angle
13. $\Gamma$	summation of four angles

With the control mass flow rate specified, the system equations consist of the twelve equations numbered 1 through 12.

A simplified version of a nonlinear block diagram for the proposed model is shown in Figure 3. Each block represents a system equation and is numbered accordingly. The output of each block can be determined when each of the indicated inputs are known. Some of the connecting lines have been omitted for simplification.

The primary feedback paths involve  $\dot{m}_r$  and  $\dot{m}_e$ . Since the entrained mass flow rate is subtracted it has a stabilizing effect on the output radius, R. Instability is caused by the positive feedback of the recirculation rate,  $\dot{m}_r$ . See Equation 8. Another feedback path results due to the effect of the radius on the volume (block 5) which in turn effects the bubble pressure (block 7). A predominant feedforward path exists through  $\dot{m}_c$  to  $\beta$  to  $V_B$  to  $P_B$ .

The input for the system is the control flow rate  $\dot{m}_c$  and represents a known function of time.

### III. NONDIMENSIONAL MODEL

It is desirable to have the modeling process be relatively independent of the exact dimensions of the amplifier and the fluid properties. For this reason, a set of nondimensional system variables is established based on the physical variables. These new quantities are:

$$[R/b], [r/b], [V_B/b^2d], [M_B/\rho b^2d], [\dot{m}_c/\dot{M}]$$

$$[\dot{m}_r/\dot{M}], [\dot{m}_e/\dot{M}], [P_B/\dot{M}^2/\rho C^2d^2], [X_r/b]$$

$$[\theta], [\beta], [\phi], [\Gamma]$$

The independent variable, time, is also made nondimensional by the following substitution.

$$T = \left( \frac{\dot{M}}{\rho b^2d} \right) t$$

Substitution of these variables into the system equations yield a new set of nondimensional equations with new coefficients. These coefficients can be collected into a set of constants which become the nondimensional parameters for the model. The nondimensional system variables  $X_i$  and parameters  $K_i$  are defined in Tables 2 and 3.

Table 2. Identification of the nondimensional system variables.

<u>Physical Variable</u>	<u>Units</u>	<u>System Variable</u>
1. $(\dot{m}_e / \dot{M})$	1	$X_1$
2. $(\dot{m}_r / \dot{M})$	1	$X_2$
3. $(\dot{m}_c / \dot{M})$	1	$X_3$ (input)
4. $(M_B / \rho b^2 d)$	1	$X_4$
5. $(P_B / \frac{\dot{M}^2}{\rho C^2 d^2})$	1	$X_5$
6. $(X_r / b)$	1	$X_6$
7. $(R / b)$	1	$X_7$
8. $(r / b)$	1	$X_8$
9. $(V_B / b^2 d)$	1	$X_9$
10. $\beta$	radians	$X_{10}$
11. $\theta$	radians	$X_{11}$
12. $\phi$	radians	$X_{12}$
13. $\Gamma$	radians	$X_{13}$

Table 3. Identification of the system parameters.

<u>Physical Constants</u>	<u>System Parameters</u>
1. $\frac{RaT}{\dot{M}^2} \rho^2 C^2 d^2 g c$	$K_1$
2. $(C/b)$	$K_2$
3. $1 - \tanh(\eta)$	$K_3$
4. $(\rho b^2 d / \dot{M}) = t/T$	$K_4$
5. $(3/4 \sigma)$	$K_5$
6. $D/b$	$K_6$
7. $\alpha$	$K_7$
8. $(\eta / \sigma)$	$K_8$
9. $(X_o/b) = \sigma / 3$	$K_9$
10. $P_\infty / (\dot{M}^2 / \rho C^2 d^2)$	$K_{10}$

The nondimensional system equations in terms of  $X_i$  and  $K_i$  are as follows:

$$X_7 \cos(K_7 + X_{10}) = X_8 \cos X_{11} + (K_6 + \frac{1}{2}) \cos K_7 - K_2 \sin K_7 \quad (13)$$

$$X_8 = X_7 - K_8 X_7 (X_{10} + X_{11} + K_7) - K_8 K_9 \quad (14)$$

$$\sin X_{12} = (\frac{1}{2} \sin X_{10}) / (X_7^2 - X_7 \cos X_{10} + 0.25)^{1/2} \quad (15)$$

$$X_{13} = X_{10} + X_{11} + X_{12} + K_7 \quad (16)$$

$$\begin{aligned} X_9 = & (\frac{1}{2}) [X_7 - 0.5 \cos(X_{10} + X_{12})]^2 X_{13} \\ & - [X_7 - \frac{1}{2} \cos(X_{10} + X_{12})] K_8 X_7 \frac{X_{13}^2}{2} + K_8^2 X_7^2 \frac{X_{13}^3}{6} \\ & - \frac{1}{2} X_8^2 \cos^2 X_{11} [\tan(X_{13} - X_{11}) + \tan X_{11}] \\ & + \frac{1}{2} [K_6 - K_2 \tan K_7]^2 \frac{[\sin(X_{10} + X_{12}) \cos K_7]}{\cos(K_7 + X_{10} + X_{12})} \end{aligned} \quad (17)$$

$$X_6 = [X_7 \sin X_{10} - K_2] / \cos K_7 + X_8 [\cos X_{11} \tan K_7 + \sin X_{11}] \quad (18)$$

$$X_5 X_9 = X_4 K_1 \quad (19)$$

$$\frac{dX_4}{dT} = X_3 + X_2 - X_1 \quad (20)$$

$$\tan X_{10} = X_3^2 / K_2 \quad (21)$$

$$\frac{(K_2)^2}{(K_9)^{1/2}} (X_{13} X_7)^{-1/2} \frac{dX_7}{dT} - (\frac{K_2}{X_7})^2 = X_5 - K_{10} \quad (22)$$

$$X_1 = [K_5 X_7 (X_{13} - X_{12}) + \frac{1}{4}]^{1/2} - \frac{1}{2} \quad (23)$$

$$X_2 = [K_5 X_7 (X_{13} - X_{12}) + \frac{1}{4}]^{1/2} K_3 \quad (24)$$

There are 13 system variables which define the state of the amplifier at any instant of time. The first three ( $X_1$ ,  $X_2$ ,  $X_3$ ) represent flow rates with  $X_3$  serving as the input to the system. The bubble mass, pressure and volume are represented by variables  $X_4$ ,  $X_5$  and  $X_9$ . Three distances within the amplifier are associated with  $X_6$ ,  $X_7$  and  $X_8$ . Finally, the last four system variables replace the angles which describe the bubble geometry.

Of the 10 system parameters listed in Table 3, the only one which has units associated with it is  $K_4$ . Since this parameter relates the model time with physical time it must have the units of time. The other nine parameters must have specific values in order to generate a solution, however,  $K_4$  is only used to convert the response time to a particular amplifier and fluid.

The 12 system equations consist of 10 algebraic equations and two differential equations. Most of the equations are nonlinear and contain cross-coupling between variables. For example, equations 13, 14 and 16 contain  $X_8$ ,  $X_{11}$  and  $X_{13}$  and a direct solution for any one of the variables is extremely difficult.

#### IV. ANALOG MODEL AND SIMULATION

The analytical model for the amplifier can now be translated into the form of an analog diagram. This diagram, shown in Figure 4, utilizes standard analog symbols which are explained in Appendix D. The flow of information and feedback paths which were present in the original block diagram are also present in the analog diagram.

Each of the system variables represents a possible output and appears somewhere on the diagram. The necessary inputs to the model are

the values for the system parameters  $K_1$ , the functional relation for the input  $X_3(T)$  and the initial values for variables  $X_4$  and  $X_7$ . As a result, both a steady state and dynamic simulation are necessary to predict the response.

#### A. Steady State Response Simulation

The steady state or equilibrium state of the amplifier is reached when the sum of all mass flows into the separation bubble is zero. In this case the bubble remains stationary and all derivatives of the system variables become zero. Thus, the system equations (Equations 13 through 24) reduce to a set of simultaneous, nonlinear algebraic equations. The steady state simulation consists of an iterating, FORTRAN program which solves these algebraic equations and predicts the equilibrium values for the 12 system variables. The inputs for the program are the control flow,  $X_3$ , and the 10 constants which depend on the amplifier geometry, fluid properties and approximate jet flow solutions.

Computer results were obtained for values of  $X_3$  ranging from 0 to 0.5. This corresponds to a control mass flow rate from 0 to 50% of the power jet mass flow rate.

In addition, two parameters  $K_2$  and  $K_6$  which are the ratios of control port width and offset distance to power nozzle width were assigned several different values. Parameters  $K_5$ ,  $K_8$  and  $K_9$  were also changed to correspond to several different values of spread parameter  $\sigma$ .

The results for two cases are shown in Figures 5 through 14. The steady state values for each of the system variables are indicated for a range of values for control input  $X_3$ .

#### B. Dynamic Response Simulation

For this portion of the response an analog simulation was sought. The system equations and block diagram lend themselves to a direct analog simulation with the nondimensional time variable  $T$  functioning as the single, independent variable. In addition, the dynamic response



of any one of the system variables might be of interest and could be easily recorded. However, because of the large number of nonlinearities present in the model an analog computer, capable of handling the problem, was not available. For this reason, an alternate means of solution was selected.

A packaged subroutine which simulates an analog computer has been developed by Lehigh University for use on the CDC 6400 digital computer. The program, referred to as LEANS, was used to provide the analog simulation for this problem. It employs the block diagram technique, commonly considered the first step of any analog simulation. The program contains a full array of integrators, summers, constants, multipliers and other nonlinear elements which can be coupled in any manner. Since the digital computer uses floating point arithmetic, time and magnitude scaling are unnecessary; and the user may program directly from the block diagram.

The LEANS simulation was prepared directly from Figure 4. The system equations were used to provide the particular functional relationships that exist between the system variables. The required inputs to this analog simulation are the numerical values for the 10 constants, initial conditions for  $X_3$ ,  $X_4$  and  $X_7$  and the final value for  $X_3$ . The input  $X_3$  was programmed to change exponentially from its initial to final value. This type of input would commonly occur in practice and has a much faster rise time than the dynamic growth of the bubble.

Results of this portion of the study are shown in Figures 15 through 36. The initial value for each system variable ( $T = 0$ ) and the final value ( $T = \infty$ ) must correspond to those values predicted by the steady state simulation. For example, in Figure 20 the initial value for  $X_7$  is 5.16 and the final value is 6.3 as  $X_3$  changes from 0.10 to 0.14. Compare these values to those shown in Figure 9 for  $X_3$  of 0.1 and 0.14.

## V. RESULTS

With the analog simulation on the computer it became possible to make a series of parametric studies. Changes in amplifier geometry, fluid conditions and input specifications could be introduced by merely changing the parameters of the simulation. Steady state results are shown in Figures 5 to 14 for two different cases. Figures 15 to 36 contain the results of the dynamic simulation for two cases A and B. The parameter values for cases A and B are given in Figures 15 and 26 respectively.

### A. Steady State Results

Entrainment and recirculated mass flow rates ( $X_1$ ,  $X_2$ ) appear in Figure 5 to be linearly dependent on the control mass flow input,  $X_3$ , but independent of parameter  $K_6$ . Bubble pressure,  $X_5$  in Figure 7, jet radius of curvature,  $X_7$  in Figure 9, and attachment radius,  $X_8$  in Figure 10, level off as the input  $X_3$  approaches 0.5. For the given range of control flow, the reattachment angle  $\theta$  decreases at first and then begins to increase. With low control flow the bubble is very small and the jet reattaches close to the supply nozzle. As a result, the reattachment angle must be somewhat larger.

### B. Dynamic Results

Results were obtained from the computer simulation for both large and small changes in input signal  $X_3$ , the ratio of mass flow from the control port to supply flow. The exponential input signal, shown in Figures 15 and 26, reaches its final value very rapidly ( $T = 3$ ).

The dynamic changes which take place in the system variables for the small signal input are shown in Figures 16 to 25. The most significant result is the change in bubble pressure ( $X_5$ ) shown in Figure 18. The model predicts a sudden decrease in pressure as the control signal is applied. The bubble pressure recovers, overshoots and finally settles down to its new equilibrium value at  $T = 15$ . The reason for this inverse response (output variable initially decreasing with an increase in input signal) is the feedforward loop

in the block diagram model (Figure 3). An increase in the input signal feeds through blocks 9, 1, 4 and 5 and has a decreasing effect on the output variables. The physical explanation is that, although an addition of control flow increases the mass in the bubble which increases the bubble pressure, it has a more direct effect of increasing the bubble volume. Due to the compressibility of air inside the bubble a decrease in bubble pressure results. This inverse response also appears in the radius of curvature for the jet (Figure 20) and the reattachment radius in Figure 21. In both cases, however, there is no overshooting of the final value.

The effect of this response could be observed through the reattachment point shown in Figure 19. For a short period of time, the reattachment point moves, very slightly, toward the supply nozzle. The bubble volume in Figure 22, on the other hand, increases continuously from its initial equilibrium value to its final value.

For this particular change in control flow the reattachment angle  $\theta$  is driven to a lower equilibrium value (see Figure 13). The angle, however, increases for a short period of time before decreasing to its final value. The dynamic response of this variable, as well as the others, takes about 15 units of  $T$  to reach its new equilibrium position. If the value of  $K_4$  (see Table 3) is known for a particular amplifier, then the total time for the response becomes  $15 K_4$  in the time units of  $K_4$ .

The dynamic response of the simulation to a large change in control flow was also sought. The sudden change in control flow variable  $X_3$  from 0.1 to 0.3 had the form shown in Figure 26. Due to the absence of side vents and a splitter the jet remains attached to the same wall but enclosing a much larger separation region. The final equilibrium position for the amplifier is reached at about  $T = 30$ . The equilibrium values for each of the system variables matches those given by the steady state simulation for  $X_3 = 0.3$  and the corresponding parameter values for  $K_1$ .

The dynamic responses of each of the system variables for this case are given in Figures 27 through 36. The same trends are evident for this case as the small input case but seem more pronounced. Bubble pressure, for example, undergoes a much larger decrease initially as shown in Figure 29. The inverse response is still present in variables  $X_6$ ,  $X_7$  and  $X_8$  as displayed in Figures 30, 31 and 32.

For the large value of control flow ( $X_3 = 0.3$ ), the final value for attachment angle is slightly larger than the initial value (see Figure 13). However, during the dynamic response the angle overshoots the value rather significantly as displayed in Figure 35. Once again it takes 30 units of  $T$  for the variable to come to equilibrium.

## VI. CONCLUSIONS

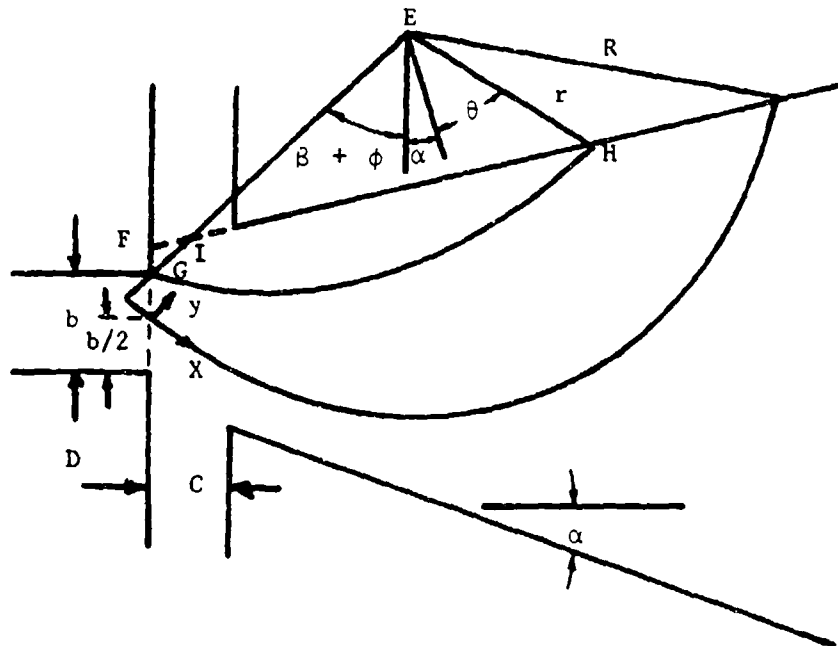
A nonlinear, dynamic model for the bubble growth within a wall attachment amplifier has been presented. Using nondimensional system variables, this model was described in analog form. From a computer simulation, the response to a sudden change in control mass flow has been studied. These results produced the following list of conclusions.

1. The separation bubble undergoes an initial decrease in pressure followed by an overshoot of its final value. If the separation region should encounter a vent during this overshooting period no mass would flow from the region through the vent.
2. For a short period of time the reattachment point moves toward the supply nozzle, before moving outward.
3. The reattachment angle undergoes a rapid increase and an overshoot of its final value. During this overshoot period the amplifier could possibly submit to a "critical angle" type of switching even though the final value for the angle does not predict it.
4. The time it takes for the amplifier to reach equilibrium (response time) is longer for a large change in control flow than for a small change.

5. The simulation results are presented in nondimensional form but with the fixed dimensions of the amplifier known, the variables can be converted to actual units. A value for the parameter  $K_4$  will convert the time scale to appropriate time units.

# APPENDIX A

The volume of the bubble, as shown in the figure below, is the product of the amplifier thickness  $d$  and the area enclosed by curve FGH. This area can be calculated by computing the large area bound by the curve FGH, subtracting the triangular portion EIH and adding the small area inside curve FIG.



Area enclosed by EGH is denoted by  $A_1$  and can be determined as follows:

$$A_1 = \int \int \rho \, d\rho \, d\lambda$$

where  $\lambda$  and  $\rho$  are the polar coordinates of a point measured from point E and line EG.

Thus,

$$A_1 = \int \frac{1}{2} \rho^2 \, d\lambda$$

and from the Goertler profile assumption:

$$\rho = R - y$$

$$y = \frac{\eta (X_1 + X)}{\sigma} = y_1 + \frac{\eta R \lambda}{\sigma}$$

Substituting

$$A_1 = \int_0^{\phi + \alpha + \beta + \theta} \left( \frac{1}{2} \right) \left[ R - \frac{\eta}{\sigma} R \lambda - y_1 \right]^2 d \lambda$$

$$A_1 = \int_0^{\phi + \alpha + \beta + \theta} \left( \frac{1}{2} \right) \left[ (R - y_1)^2 - 2(R - y_1) \left( \frac{\eta R}{\sigma} \right) \lambda + \left( \frac{\eta R \lambda}{\sigma} \right)^2 \right] d \lambda$$

$$A_1 = \left( \frac{1}{2} \right) (R - y_1)^2 \Gamma - (R - y_1) \frac{\eta R}{\sigma} \frac{\Gamma^2}{2} + \left( \frac{\eta R}{\sigma} \right)^2 \frac{\Gamma^3}{6}$$

where

$$\Gamma = \phi + \alpha + \beta + \theta$$

$$y_1 = \left( \frac{1}{2} \right) b \cos (\beta + \phi)$$

The areas of the two large triangles are  $A_2$  and  $A_3$  and can be easily calculated.

$$A_2 = \frac{1}{2} (r \sin \theta) (r \cos \theta)$$

$$A_3 = \frac{1}{2} [r \cos (\theta) \tan (\phi + \beta + \alpha)] [r \cos \theta]$$

The small triangle FIG has area  $A_4$  where

$$A_4 = \frac{1}{2} [D - C \tan \alpha]^2 \left[ \frac{\sin (\beta + \phi) \sin (90 + \alpha)}{\sin (90 - \alpha - \rho - \phi)} \right]$$

Finally, the bubble volume can be calculated combining the four areas.

$$V_B = d[A_1 - A_2 - A_3 + A_4]$$

$$\begin{aligned} V_B = d \{ & \frac{1}{2} (R - y_1)^2 \Gamma - (R - y_1) \frac{\eta R}{\sigma} \frac{\Gamma^2}{2} + \left(\frac{\eta R}{\sigma}\right)^2 \frac{\Gamma^3}{6} \\ & - \frac{1}{2} [r^2 \cos^2 \theta (\tan \theta + \tan(\phi + \delta + \alpha))] \\ & + \frac{1}{2} [D - C \tan \alpha]^2 \left[ \frac{\sin(\beta + \phi) \sin(90 + \alpha)}{\sin(90 - \alpha - \beta - \phi)} \right] \} \end{aligned}$$



## APPENDIX B

The relationship between power jet radius,  $R$ , and the pressure difference across the jet can be obtained by writing the momentum equation in the  $r$  direction.

$$\frac{\partial V_r}{\partial t} + V_r \frac{\partial V_r}{\partial r} + \frac{V_\phi}{r} \frac{\partial V_r}{\partial \phi} - \frac{V_\phi^2}{r} = \frac{-1}{\rho} \frac{\partial P}{\partial r}$$

Assuming  $V_r$  is independent of  $\phi$  and  $t$ ,

$$V_r \frac{\partial V_r}{\partial r} - \frac{V_\phi^2}{r} = \frac{-1}{\rho} \frac{\partial P}{\partial r}$$

substituting,

$$r = R + y$$

$$V_r = \frac{dR}{dt} + V_y$$

one obtains the following,

$$\left( \frac{dR}{dt} + V_y \right) \frac{\partial V_y}{\partial y} - \frac{V_\phi^2}{(R + y)} = \frac{-1}{\rho} \frac{\partial P}{\partial y}$$

noting that  $\frac{dR}{dt} > V_y$  and  $R \gg y$  and neglecting terms the following equation results.

$$\frac{dR}{dt} \left( \frac{\partial V_y}{\partial y} \right) - \frac{V_\phi^2}{R} = \frac{-1}{\rho} \frac{\partial P}{\partial y}$$

Integrating with respect to  $y$  from  $+\infty$  to  $-\infty$ ,

$$\left( \int_{-\infty}^{+\infty} \rho \frac{\partial V_y}{\partial y} dy \right) \frac{dR}{dt} - \frac{J_s}{R} = (P_B - P_\infty)$$

where  $J_s$  is the power jet momentum,  $P_B$  is the bubble pressure and  $P_\infty$  is the pressure on the opposite side of the jet. This is the familiar jet curvature equation with an additional term that depends on  $\frac{dR}{dt}$ . For the steady state case ( $\frac{dR}{dt} = 0$ ) it reduces to the simpler curvature expression. The integral can be completed with this result.

$$\rho V_y \int_{-\infty}^{+\infty} \frac{dR}{dt} - \frac{J_s}{R} = P_B - P_\infty$$

Assuming that velocity  $V_y$  has the Goertler distribution,

$$\left\{ \frac{3 \rho J_s}{16 X \sigma} \right\}^{1/2} \left\{ \frac{8 \eta}{(e^\eta - e^{-\eta})^2} - \tanh \eta \right\} \int_{-\infty}^{+\infty} \frac{dR}{dt} - \frac{J_s}{R} = P_B - P_\infty$$

a differential equation is obtained which has a coefficient that depends on the position along the jet centerline,  $X$ . The supply jet velocity is noted by  $U_s$ .

$$\rho \frac{U_s}{\sigma} \sqrt{\frac{X_o}{X}} \frac{dR}{dt} - \frac{J_s}{R} = P_B - P_\infty$$

The average value of this coefficient will be determined as  $X$  varies from zero to its maximum value of  $R \Gamma$ ,

$$\begin{aligned} C_{ax,y} &= \left( \frac{1}{R \Gamma} \right) \int_0^{R \Gamma} \frac{\rho U_s}{\sigma} \sqrt{\frac{X_o}{X}} dx \\ &= \frac{1}{R \Gamma} \left[ 2 \rho \frac{U_s}{\sigma} X_o \sqrt{\frac{R \Gamma}{X_o}} \right] \end{aligned}$$

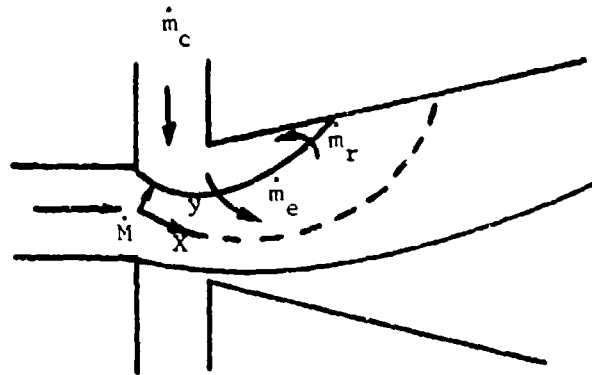
$$= 2 \rho \frac{U_B}{\sigma} \sqrt{\frac{x_o}{R \Gamma}}$$

where  $\Gamma$  is the total angle swept out by the bubble. Using this expression and writing the supply jet velocity and momentum in terms of the mass flow from the supply nozzle ( $\dot{M}$ ), the following equation is obtained.

$$\frac{\dot{M}}{b d \sigma} \sqrt{\frac{x_o}{R \Gamma}} \left( \frac{dR}{dt} \right) - \frac{M^2}{\rho b d^2} \left( \frac{1}{R} \right) = P_B - P_\infty$$

## APPENDIX C

The bubble region shown in the figure below is assumed to have a uniform pressure. Mass is being added to the region from the control port at a rate  $\dot{m}_c$ . The main jet entrains mass from the region at a rate  $\dot{m}_e$  and recirculates mass at a rate  $\dot{m}_r$ .



### (1) Entrained mass flow rate

The total entrainment at some point X is obtained by calculating the total mass flow on the bubble side of the jet and subtracting one half of the inlet flow rate.

$$\dot{m}_{ex} = \rho d \int_0^{j.b.} u dy - 0.5 \dot{M} \quad \text{where j.b. indicates the jet boundary}$$

Using the Goertler distribution,

$$\dot{m}_{ex} = \rho d \int_0^{\infty} \left( \frac{3\dot{M}^2 \sigma}{4 \rho^2 X d^2 b} \right)^{1/2} \frac{X}{\sigma} \text{sech}^2 \eta d \eta - 0.5 \dot{M}$$

$$\dot{m}_{ex} = \dot{M} \left( \frac{3X}{4b\sigma} \right)^{1/2} \int_0^{\infty} \text{sech}^2 \eta d \eta - 0.5 \dot{M}$$

$$\dot{m}_{ex} = \dot{M} \left( \frac{3X}{4b\sigma} \right)^{1/2} - 0.5 \dot{M}$$

The total entrainment along the entire edge of the bubble is desired. Substituting,

$$X = R( \beta + \alpha + \theta ) + X_0$$

$$X_0 = \frac{\sigma b}{3}$$

results in the following:

$$\dot{m}_e = \dot{M} \left( \frac{3R}{4b\sigma} ( \beta + \alpha + \theta ) + \frac{1}{4} \right)^{1/2} - 0.5 \dot{M}$$

## (2) Recirculated mass flow rate

The total amount of mass that recirculates into the bubble can be calculated by integrating the velocity profile between the attaching streamline ( $\eta$ ) and  $+\infty$  at the attachment point. This point is defined by this attaching streamline and the boundary of the amplifier.

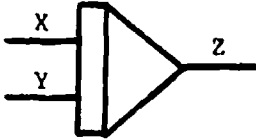
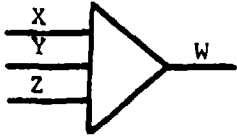
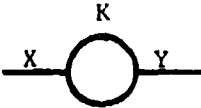
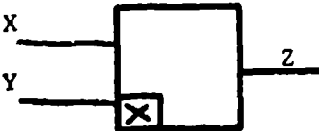
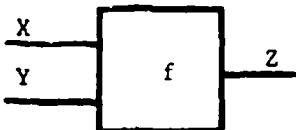
$$\begin{aligned} \dot{m}_r &= \rho \int_{Y_e}^{\infty} \int_0^d u dy dz \\ \dot{m}_r &= \rho d \int_{\eta}^{\infty} \left( \frac{3\dot{M}^2 X}{\rho^2 d^2 b \sigma^4} \right)^{1/2} \text{sech}^2 \eta d\eta \\ \dot{m}_r &= \dot{M} \left( \frac{3X}{4\sigma b} \right)^{1/2} (1 - \tanh \eta) \end{aligned}$$

Substituting for X

$$\dot{m}_r = \dot{M} \left[ \frac{3R}{4b\sigma} ( \beta + \alpha + \theta ) + \frac{1}{4} \right]^{1/2} (1 - \tanh \eta)$$

## APPENDIX D

This appendix contains a list of the standard analog elements and their corresponding mathematical operations.

<u>Element</u>	<u>Symbol</u>	<u>Mathematical Operation</u>
Integrator		$Z = \int_0^t (X+Y) dt$
Summer		$W = X + Y + Z$
Attenuator		$Y = KX$
Multiplier		$Z = XY$
Nonlinear Function		$Z = f(X, Y)$

### Acknowledgement

This work was supported by Project: "Fluid Amplifiers" monitored by Mr. David S. Siegel of the Office of Naval Research, code 461, contract number N00014-69-A-0417. The author wishes to express his thanks to Dr. Jerzy A. Owczarek and Dr. Alan H. Stenning for their helpful comments and suggestions throughout this study.

## REFERENCES

1. Bourque, C. and Newman, B. G., "Reattachment of a Two-Dimensional, Incompressible Jet to an Adjacent Flat Plate", Aero. Quarterly, Vol. 11, August 1960.
2. Brown, F. T., "Pneumatic Pulse Transmission with Bi-Stable Jet Relay Reception and Amplification", ScD. Thesis, Mechanical Engineering Dept., Massachusetts Institute of Technology, May 1962.
3. Sawyer, R. A., "The Flow Due to a Two-Dimensional Jet Issuing Parallel to a Flat Plate", Journal of Fluid Mechanics, Vol. 9, Part 4, December 1960.
4. Perry, C. C., "Two-Dimensional Jet Attachment", Advances in Fluidics, ASME, May 1967.
5. Sher, N. C., "Jet Attachment and Switching in Bistable Fluid Amplifiers", ASME Paper 64-FE-19, May 1964.
6. Levin, S. G. and Manion, F. M., "Jet Attachment Distance as a Function of Adjacent Wall Offset and Angle", HDL Report TR-1087, December 1962.
7. McRee, D. I. and Moses, H. L., "The Effect of Aspect Ratio and Offset on Nozzle Flow and Jet Reattachment", Advances in Fluidics, ASME, May 1967.
8. Mueller, T. J., "An Experimental Investigation of the Reattachment of Compressible Two-Dimensional Jets", ASME Paper 64-FE-18, May 1964.
9. Hrubecky, H. F. and Pierce, L. N., "The Effects of Geometric Changes Upon the Switching Point in a Model Bi-Stable Fluid Amplifier", Symposium on Fluid Amplification, Harry Diamond Laboratories, May 1964.
10. Steptoe, B. J., "Steady State and Dynamic Characteristic Variations in Digital Wall-Attachment Devices", Paper B3, Second Cranfield Fluidics Conference, January 1967.
11. Muller, H. R., "A Study of the Dynamic Features of a Wall Reattachment Fluid Amplifier", ASME Paper 64-FE-10.
12. Katz, S., Winston, E. T., and Howes, P., "The Response of a Bistable Fluid Amplifier to a Step Input", Proceedings of the Fluid Amplification Symposium, HDL, Vol. 1, May 1964.



13. Wilson, M. P., "The Switching Process in Bistable Fluid Amplifiers", ASME Paper 69-Flcs-28.
14. Savkar, S. D., Hansen, F. H., and Keller, R. B., "Experimental Study of Switching in a Bistable Fluid Amplifier", ASME Paper 67-WA/FE-37.
15. Kirshner, J. M., Fluid Amplifiers, McGraw Hill, New York, 1960.
16. Lush, P. A., "A Theoretical and Experimental Investigation of the Switching Mechanism in a Wall Attachment Fluid Amplifier", Proceedings IFAC Symposium on Fluidics, November 1968.
17. Lush, P. A., "Investigation of the Switching Mechanism in a Large Scale Model of a Turbulent Reattachment Amplifier", Second Cranfield Fluidics Conference, Paper A1, January 1967.
18. Harvey, D. W., "Transient Theory of Switching in a Bistable Valve", Proceedings of the Fluid Amplification Symposium, HDL, Vol. 4, 1965.
19. Sarphaja, T., "Steady and Transient Behavior of a Bistable Fluid Amplifier to a Step Input", Proceedings of the Fluid Amplification Symposium, HDL, Vol. 1, May 1964.
20. Desai, P. V. and Hrubecsky, H. F., "Dynamic Behavior of a Switching Jet in a Model Bistable Fluidic Device", ASME Paper 70-WA/Flcs-20.
21. Epstein, M., "Theoretical Investigation of the Switching Mechanism in a Bistable Wall Attachment Fluid Amplifier", ASME Paper 70-Flcs-3.
22. Ozgü, M. R. and Stenning, A. H., "Switching Dynamics of a Bistable Fluidic Amplifiers with Low Setbacks", ASME Paper 71-WA/Flcs-8.
23. Moses, H. L. and McRee, D. J., "Switching in Digital Fluid Amplifiers", ASME Paper 69-Flcs-51.
24. Ozgü, M. R. and Stenning, A. H., "Theoretical Study of the Switching Dynamics of Bistable Fluidic Amplifier with Low Setbacks", ASME Paper 71-WA/Flcs-6.

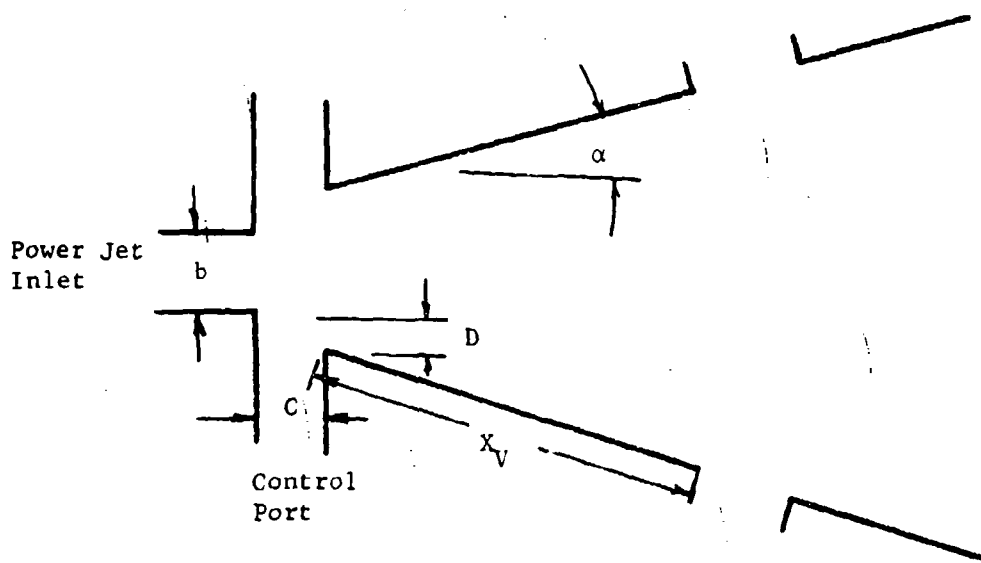


Figure 1. Geometry of the Bistable Amplifier.

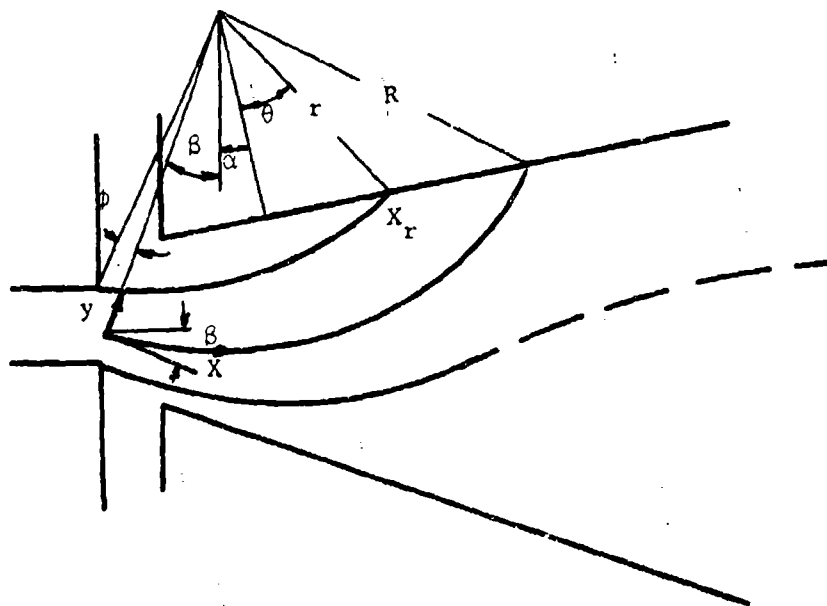


Figure 2. Geometry of the Attached Jet.

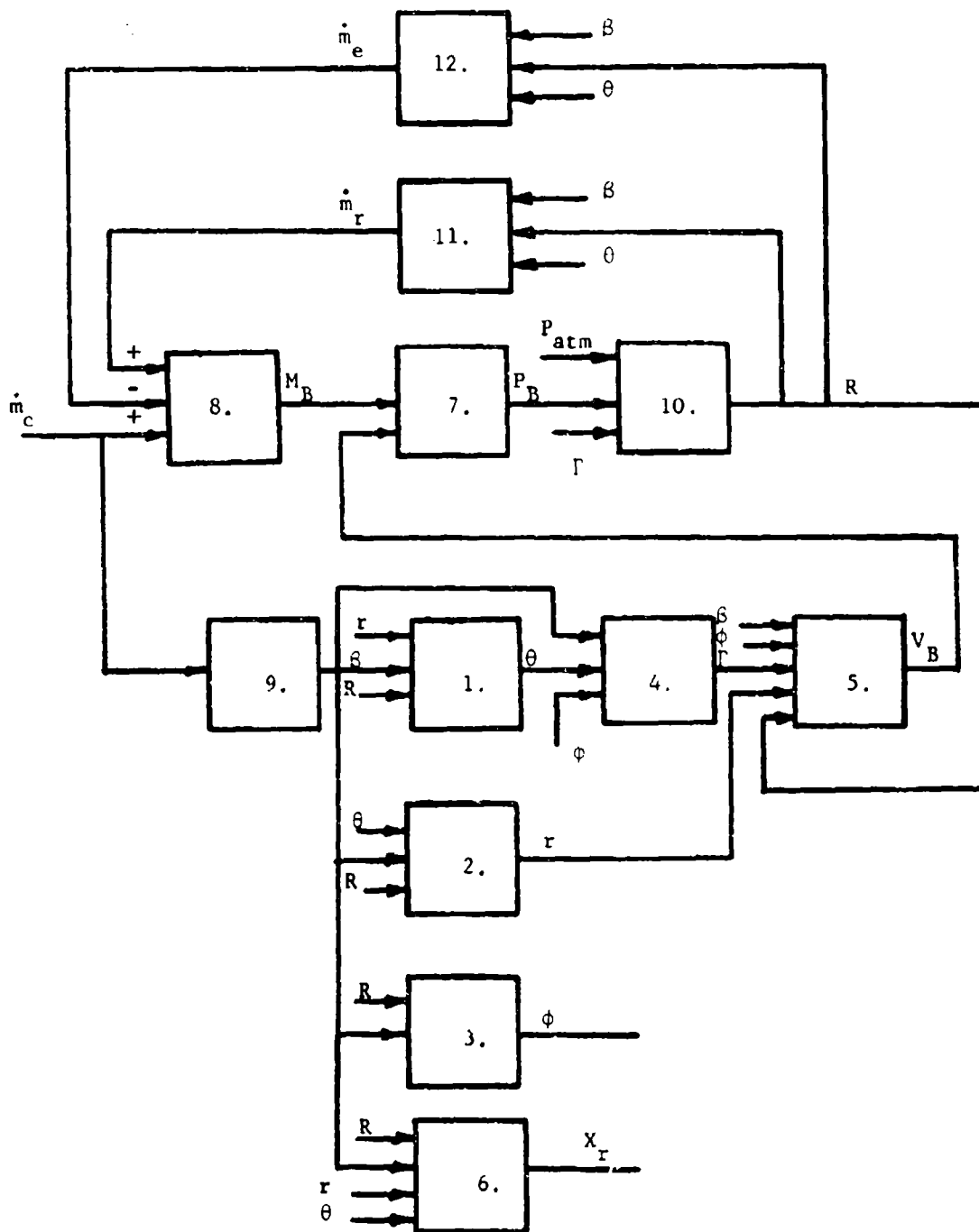


Figure 3. Block Diagram for the Amplifier in Physical Variables.

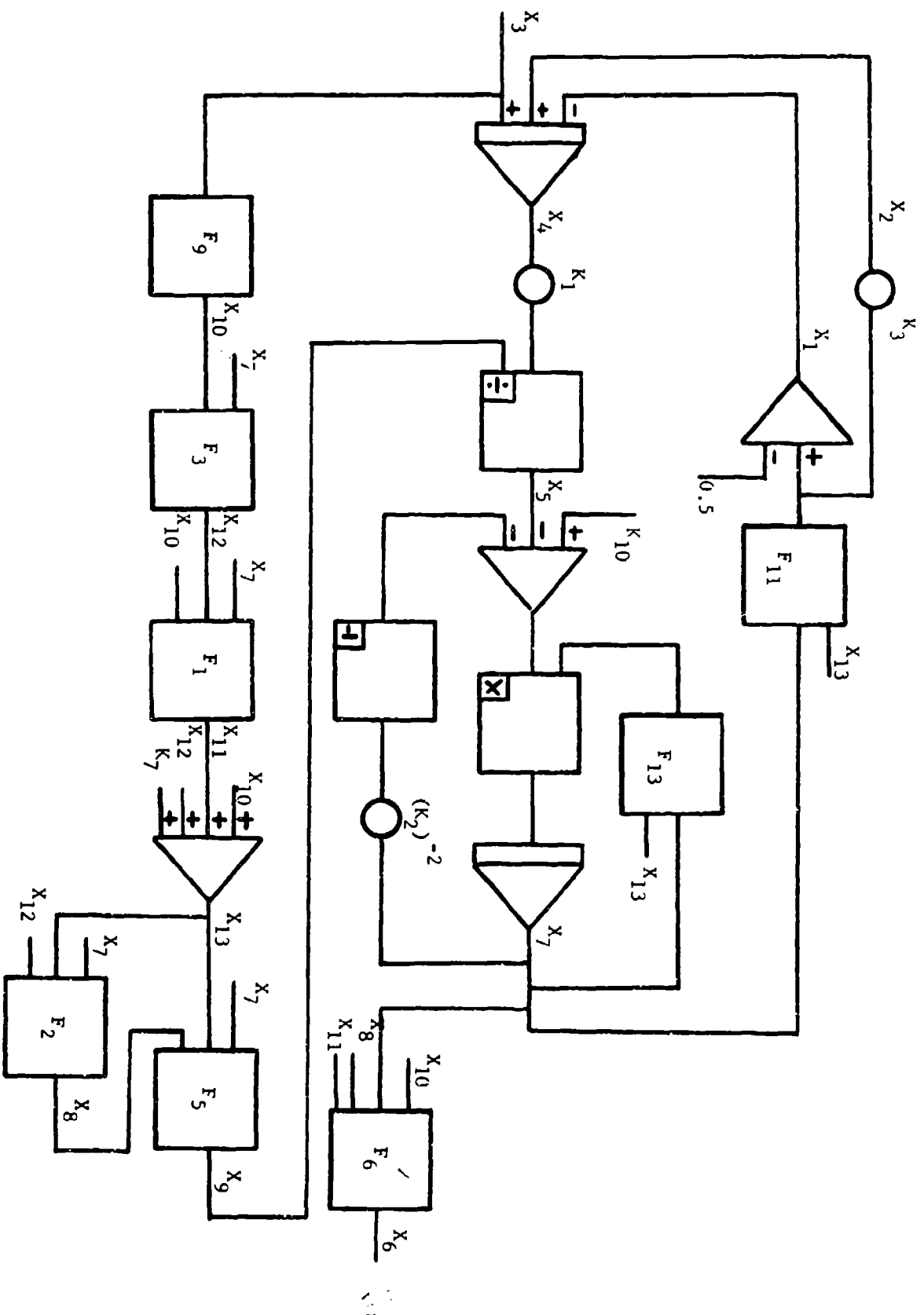


Figure 4. Analog Diagram for the Amplifier in Nondimensional System Variables.

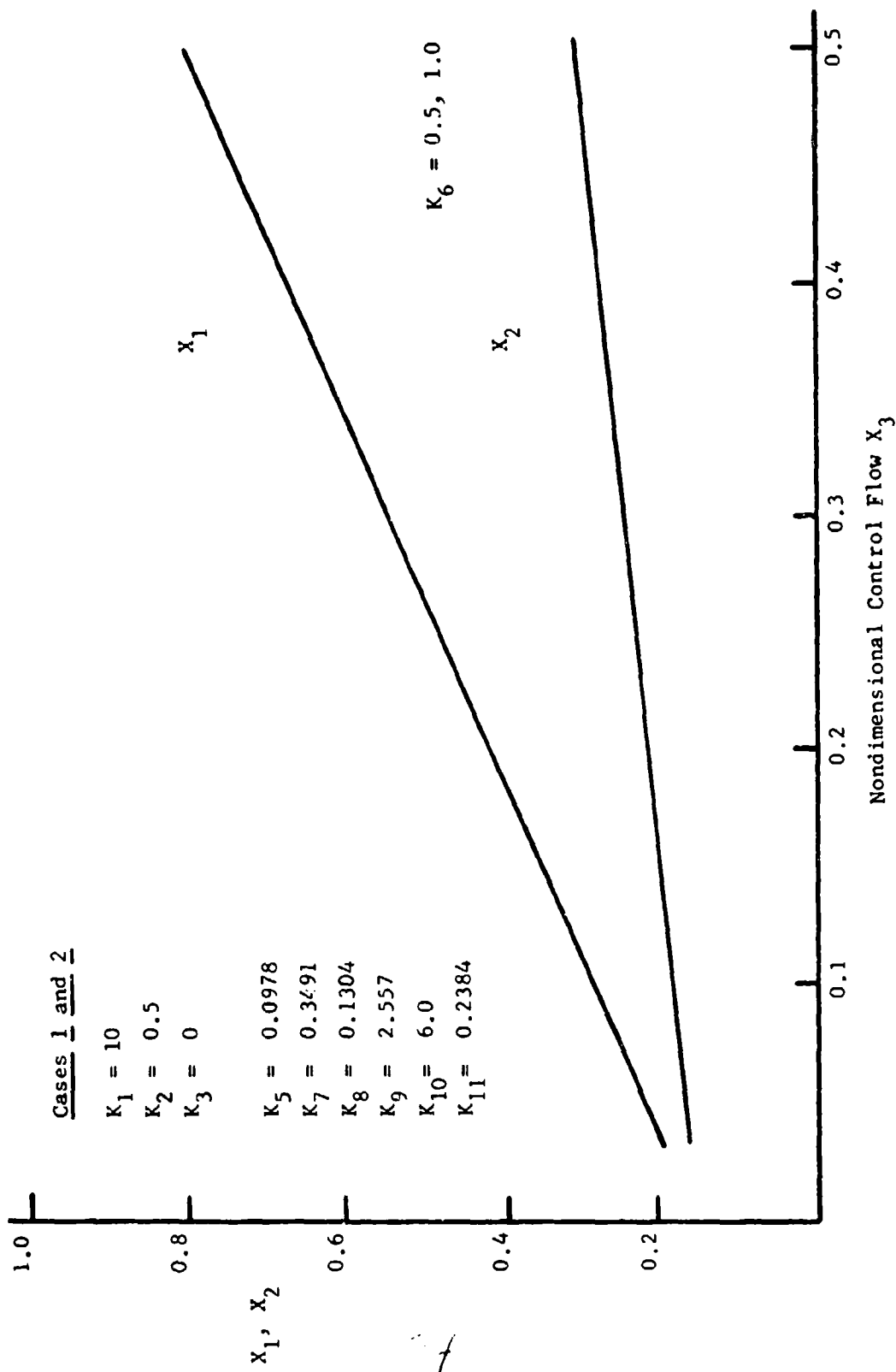


Figure 5. Steady State Results for the Entrainment and Recirculating Mass Flows ( $x_1$ ,  $x_2$ ).

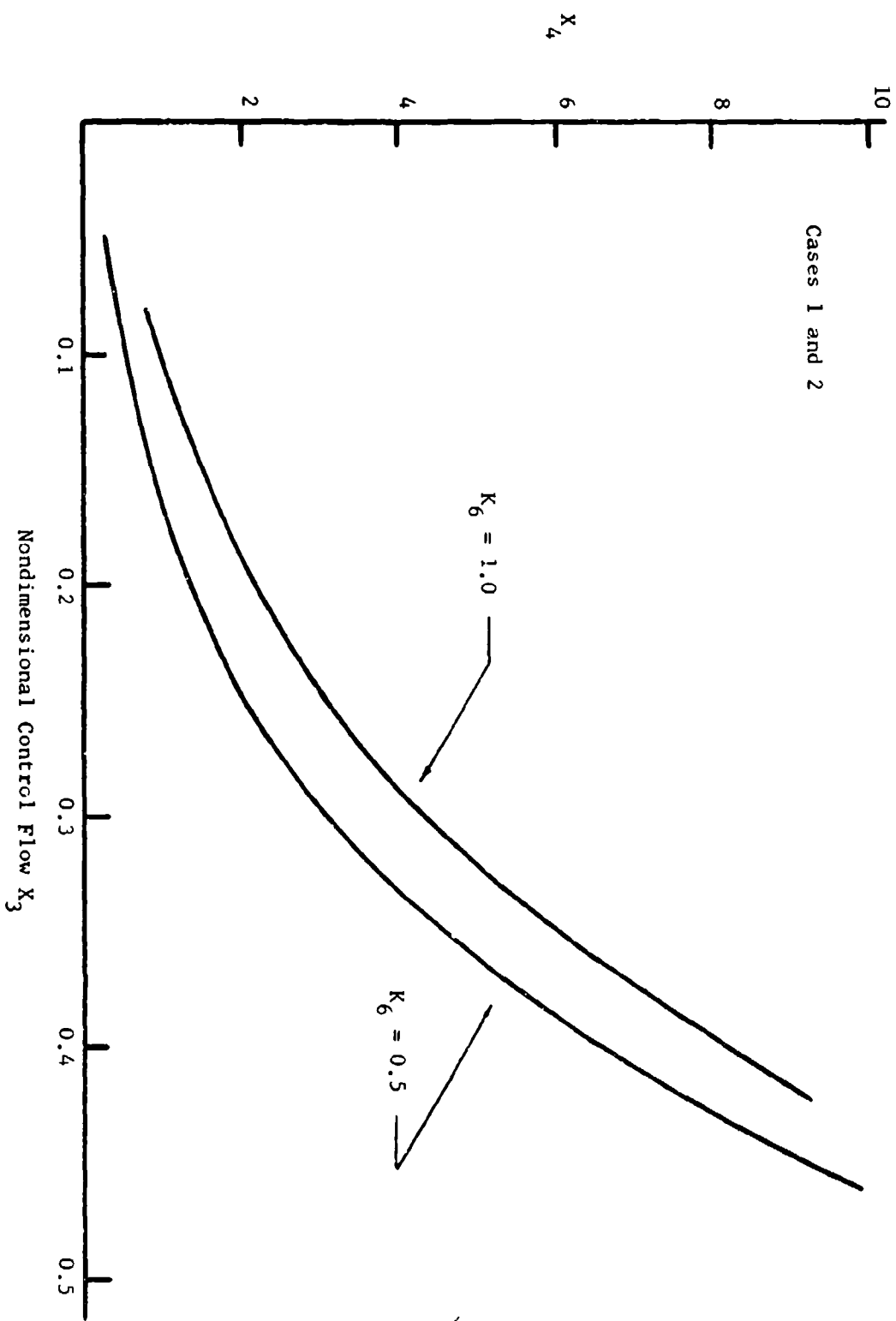


Figure 6. Steady State Results for the Bubble Mass ( $X_4$ ).

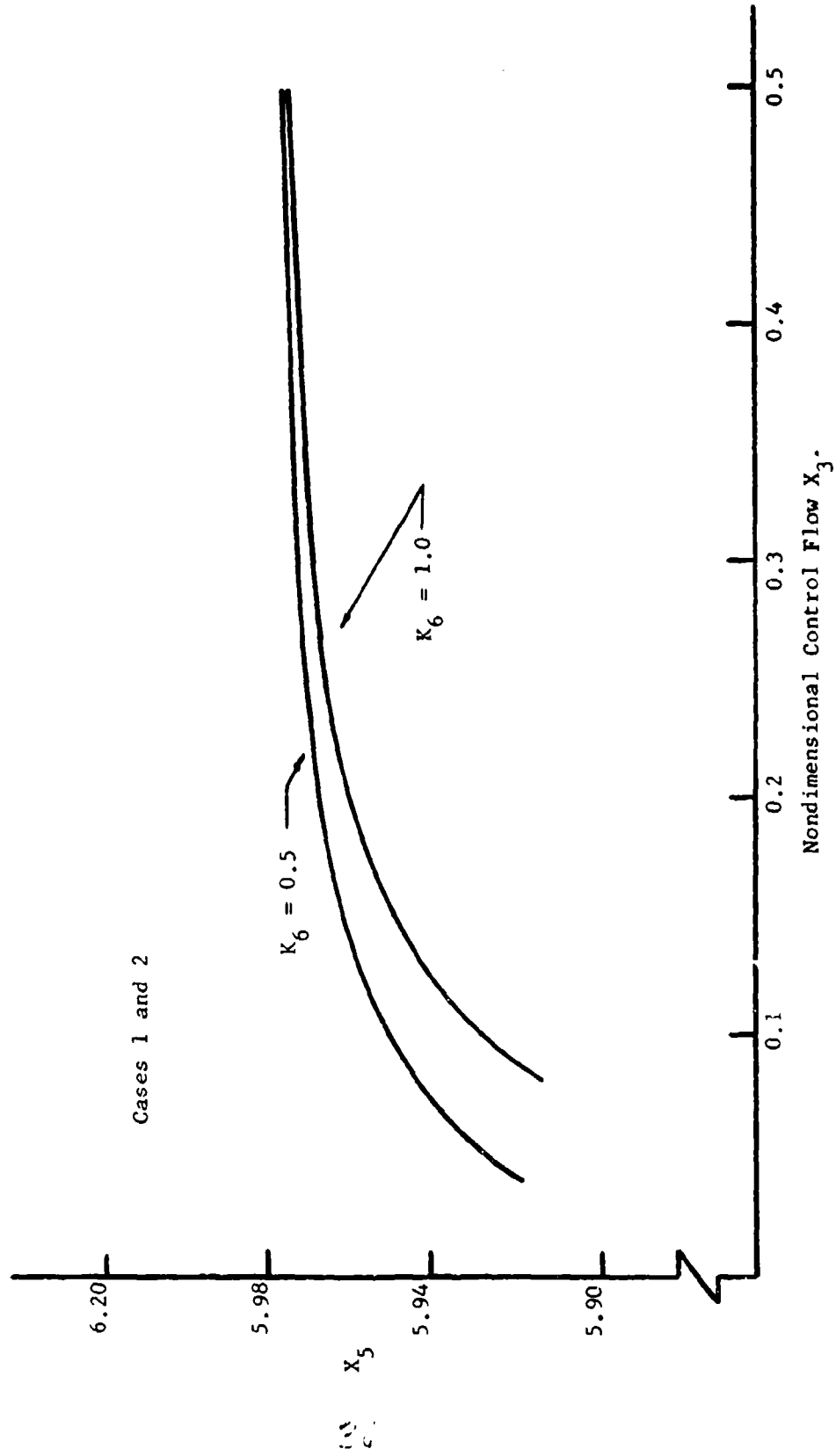


Figure 7. Steady State Results for the Bubble Pressure ( $X_5$ ).

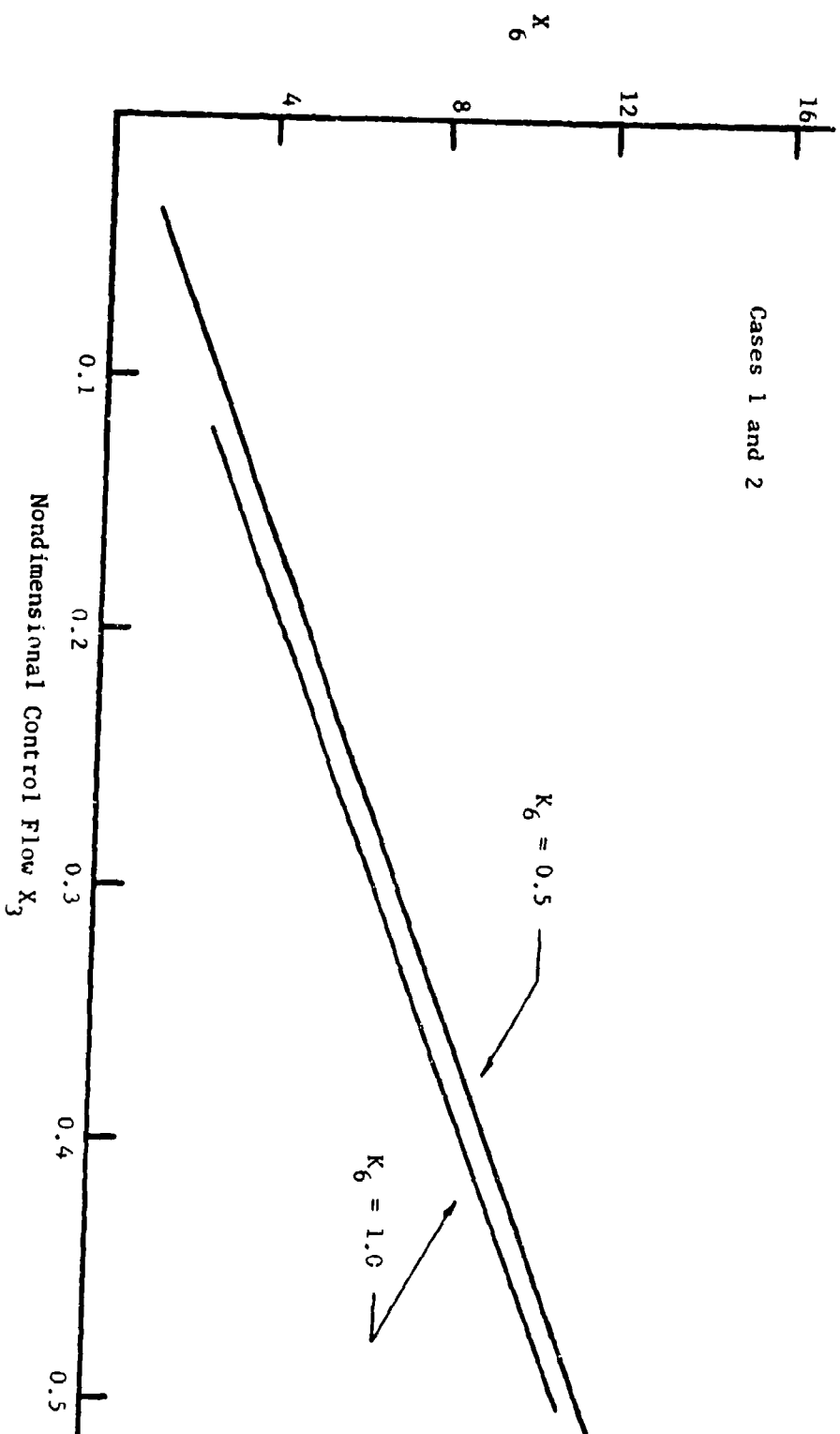


Figure 8. Steady State Results for the Reattachment Length ( $X_6$ ).



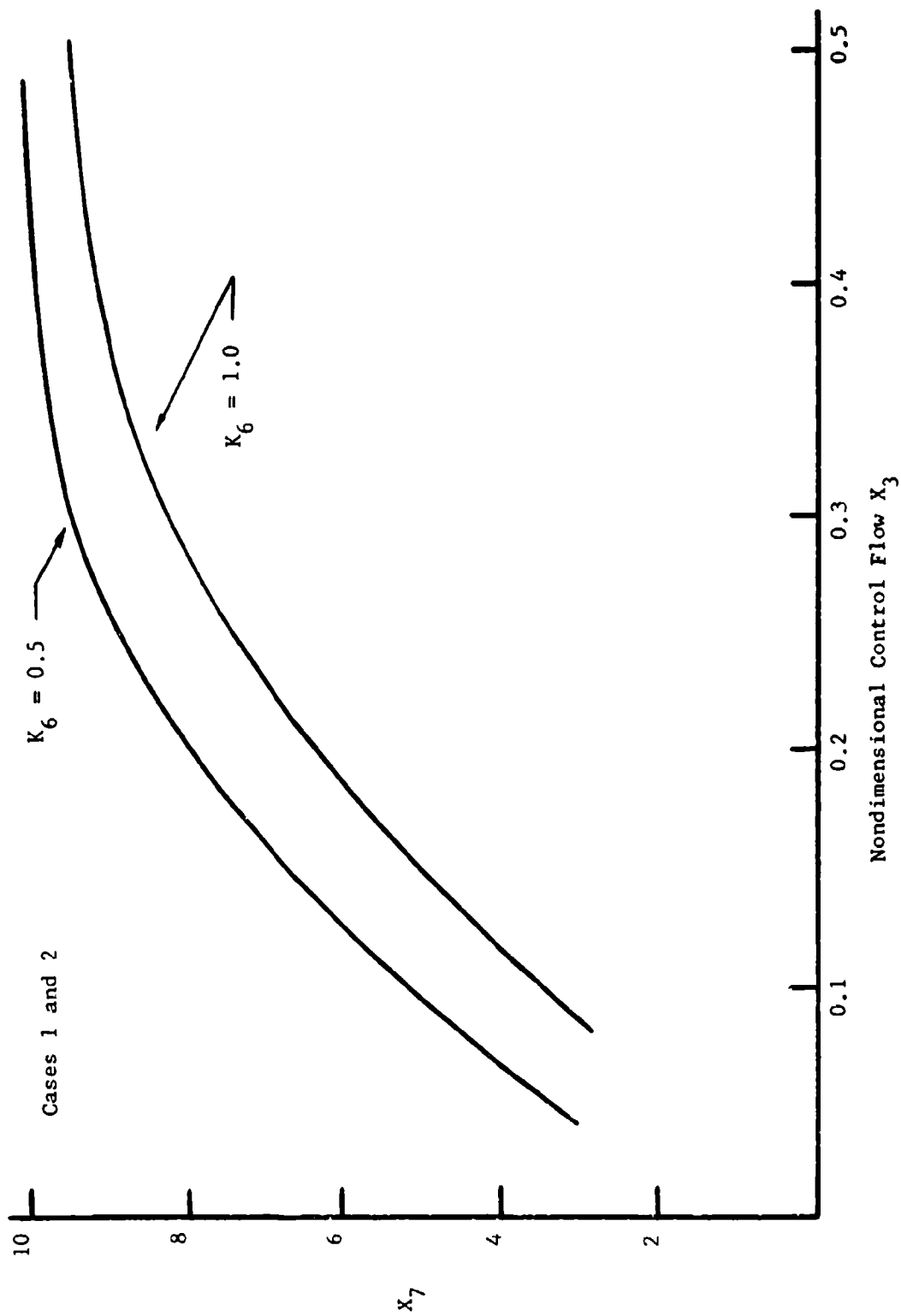


Figure 9. Steady State Results for Jet Radius of Curvature ( $X_7$ ).

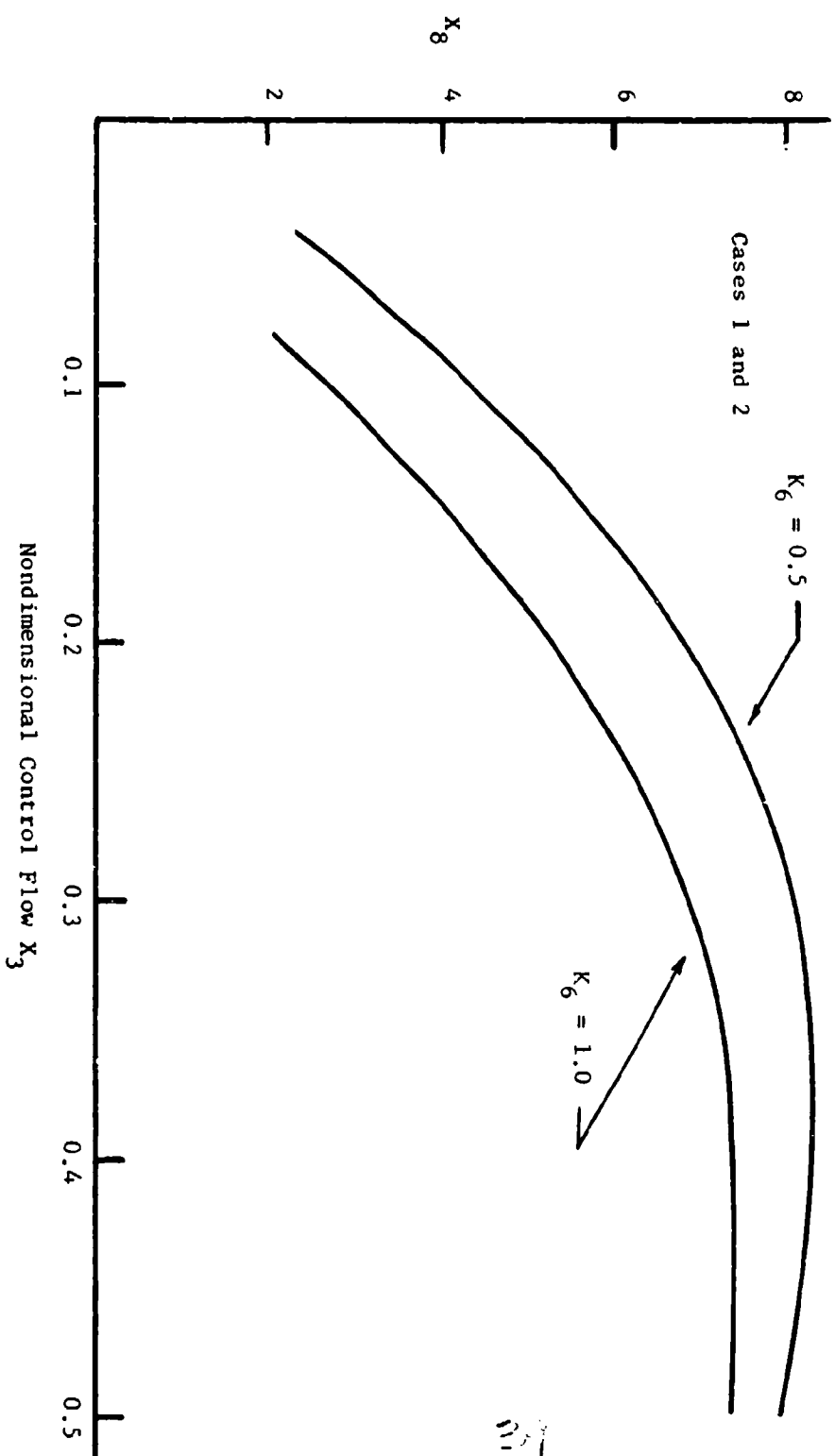


Figure 10. Steady State Results for Reattachment Radius ( $x_8$ ).

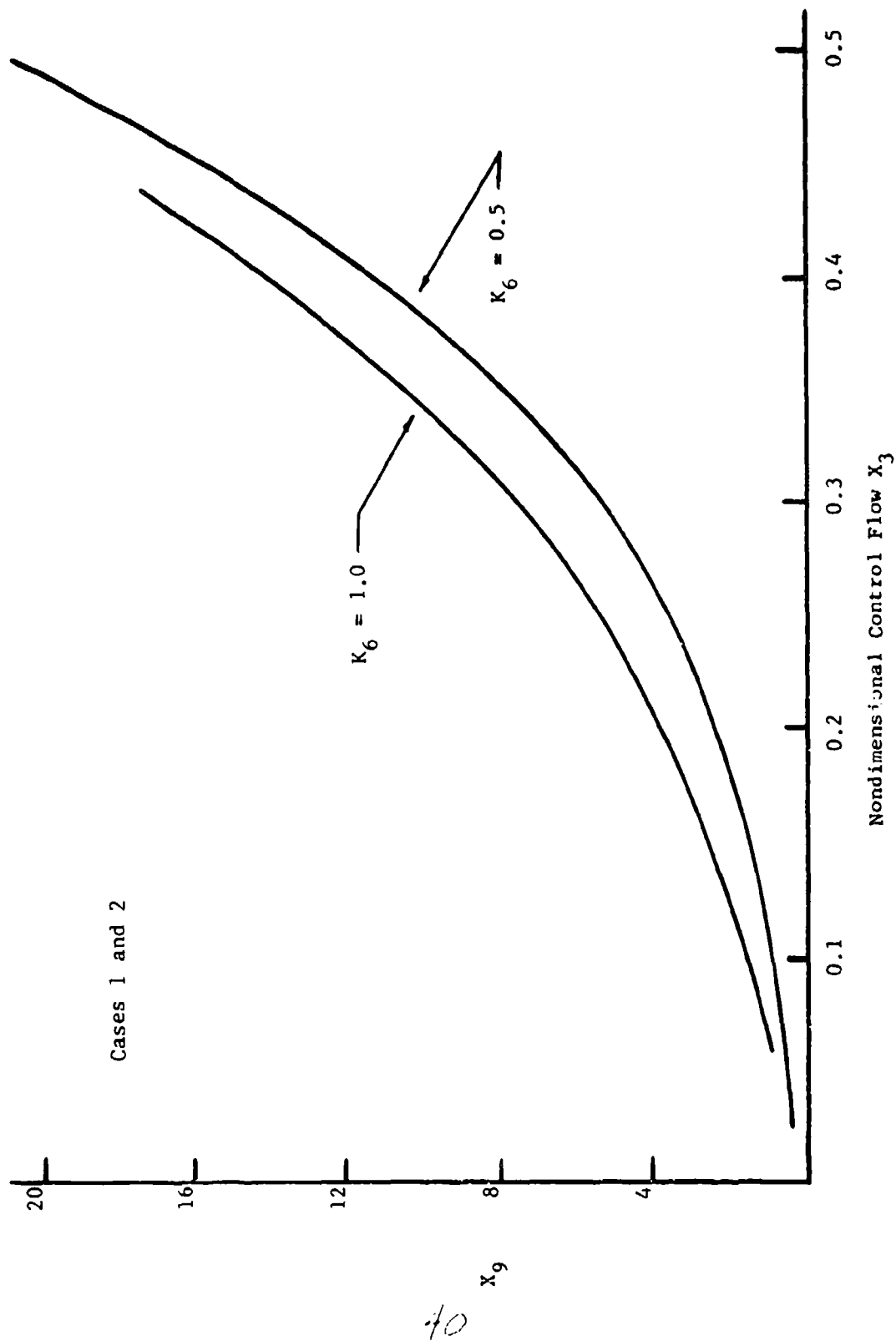


Figure 11. Steady State Results for Bubble Volume ( $x_9$ ).

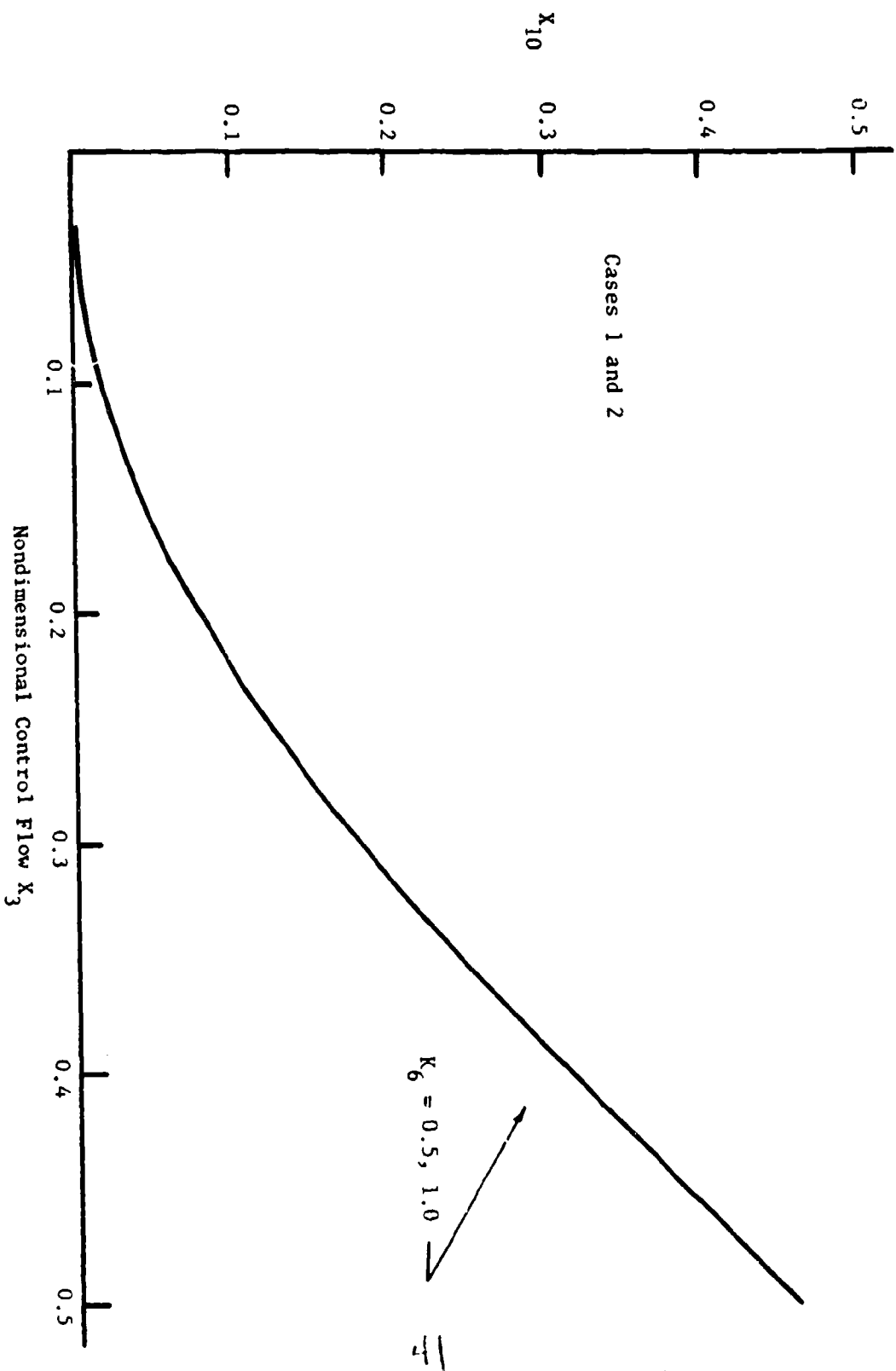


Figure 12. Steady State Results for Angle  $\beta$  ( $X_{10}$ ).

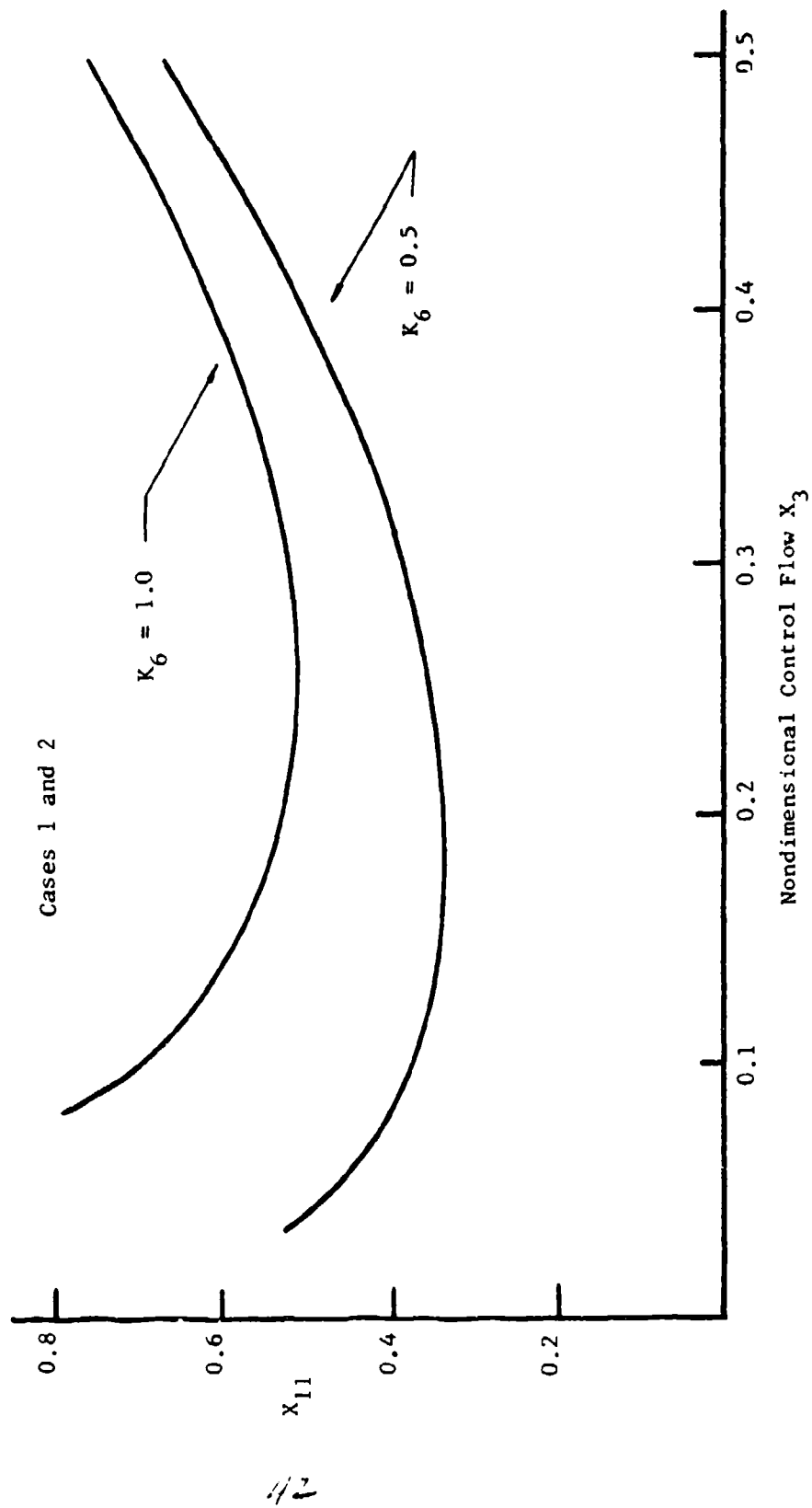


Figure 13. Steady State Results for Angle  $\theta$  ( $x_{11}$ ).

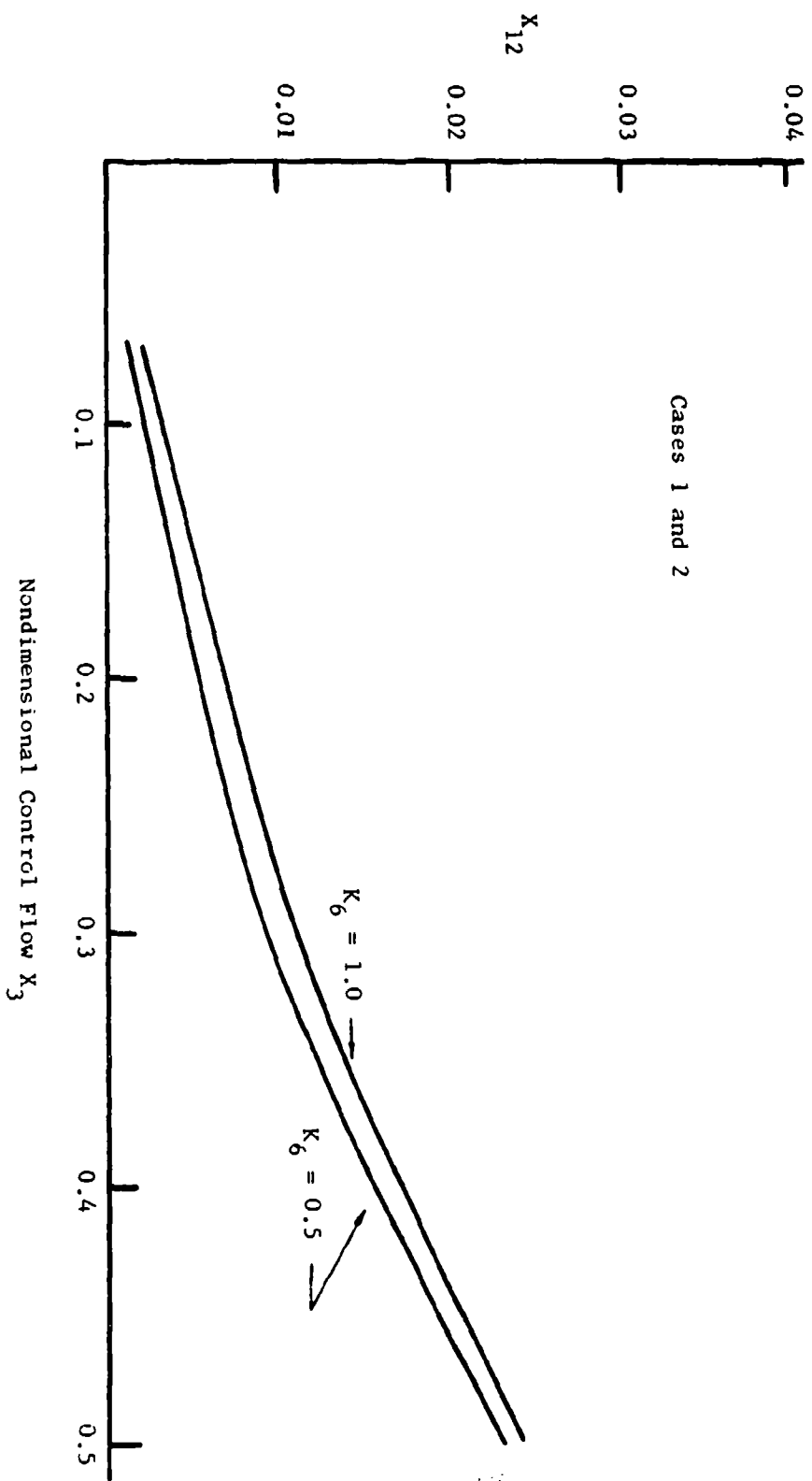


Figure 14. Steady State Results for Angle  $\phi$  ( $X_{12}$ ).

Case A

$K_1 = 10$   
 $K_2 = 0.5$   
 $K_3 = 1.0$   
 $K_5 = 0.0976$   
 $K_6 = 0.5$

$K_7 = 0.3491$   
 $K_8 = 0.1304$   
 $K_9 = 2.537$   
 $K_{10} = 6.0$   
 $K_{11} = 0.2324$

$X_3(0) = 0.10$   
 $X_3(\infty) = 0.14$

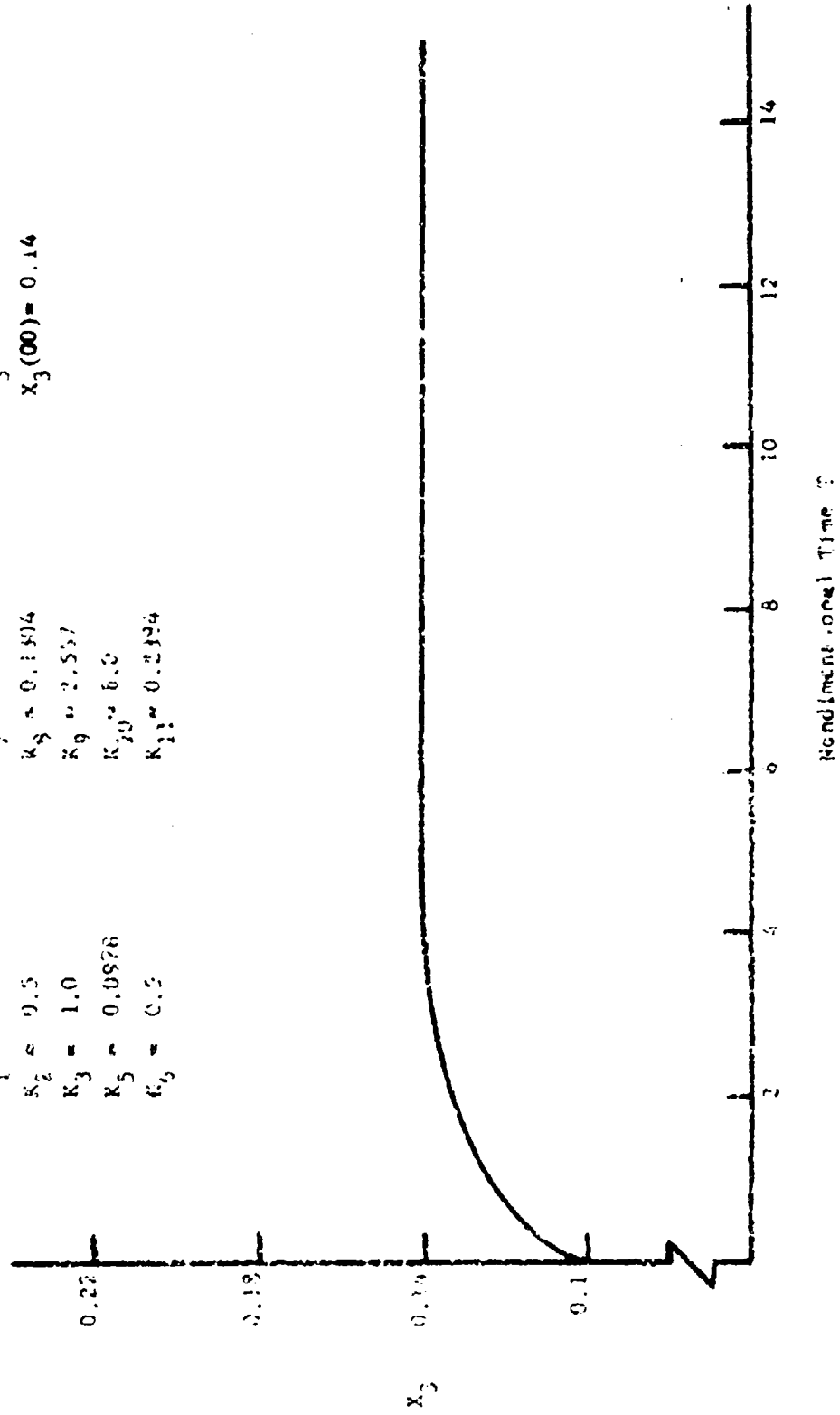


Figure 15. Dynamic Input for Case A - Small Change in Control Flow ( $X_3$ ).

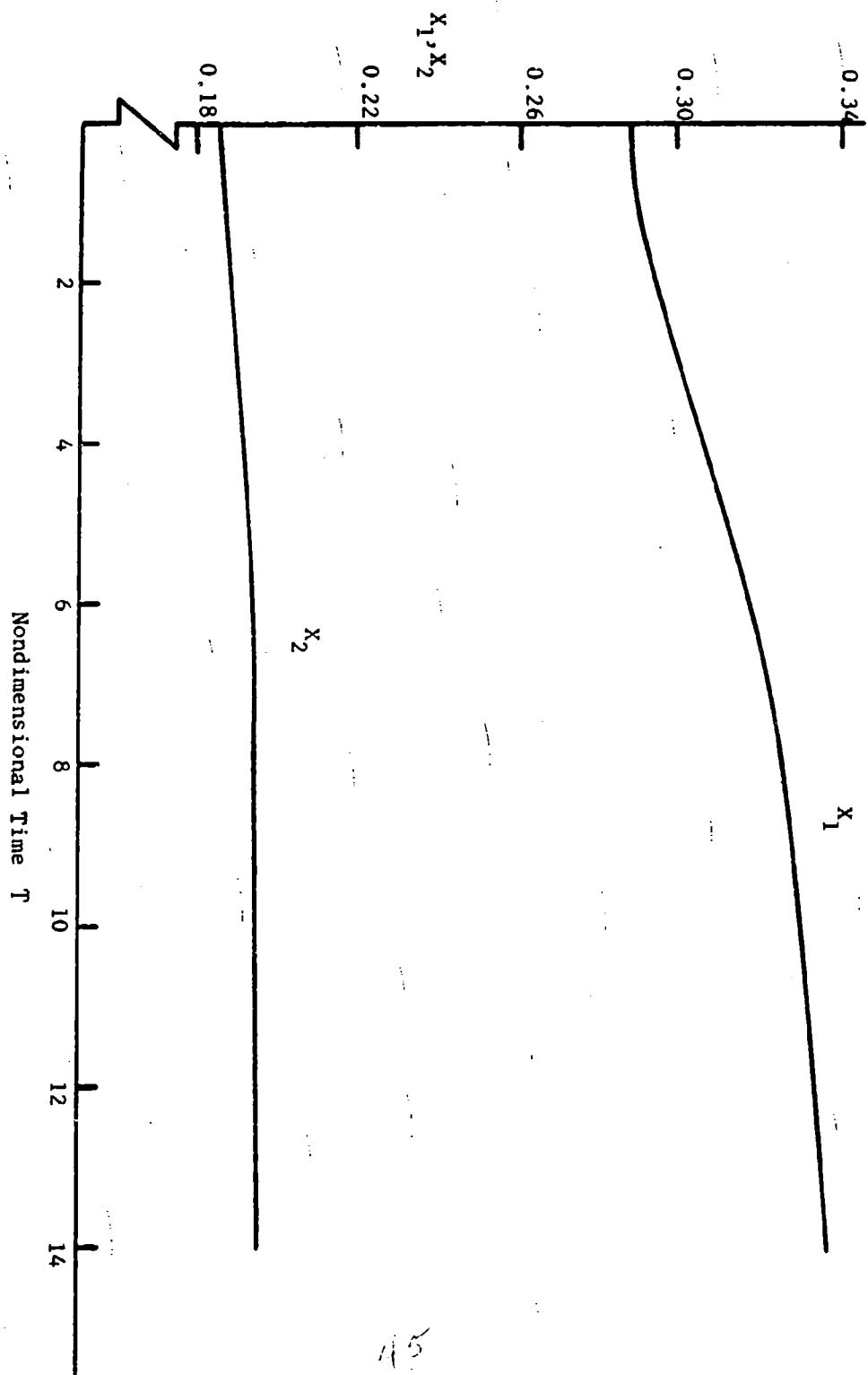


Figure 16. Dynamic Response of Entrainment and Recirculating Flows ( $X_1$ ,  $X_2$ ) for Case A.



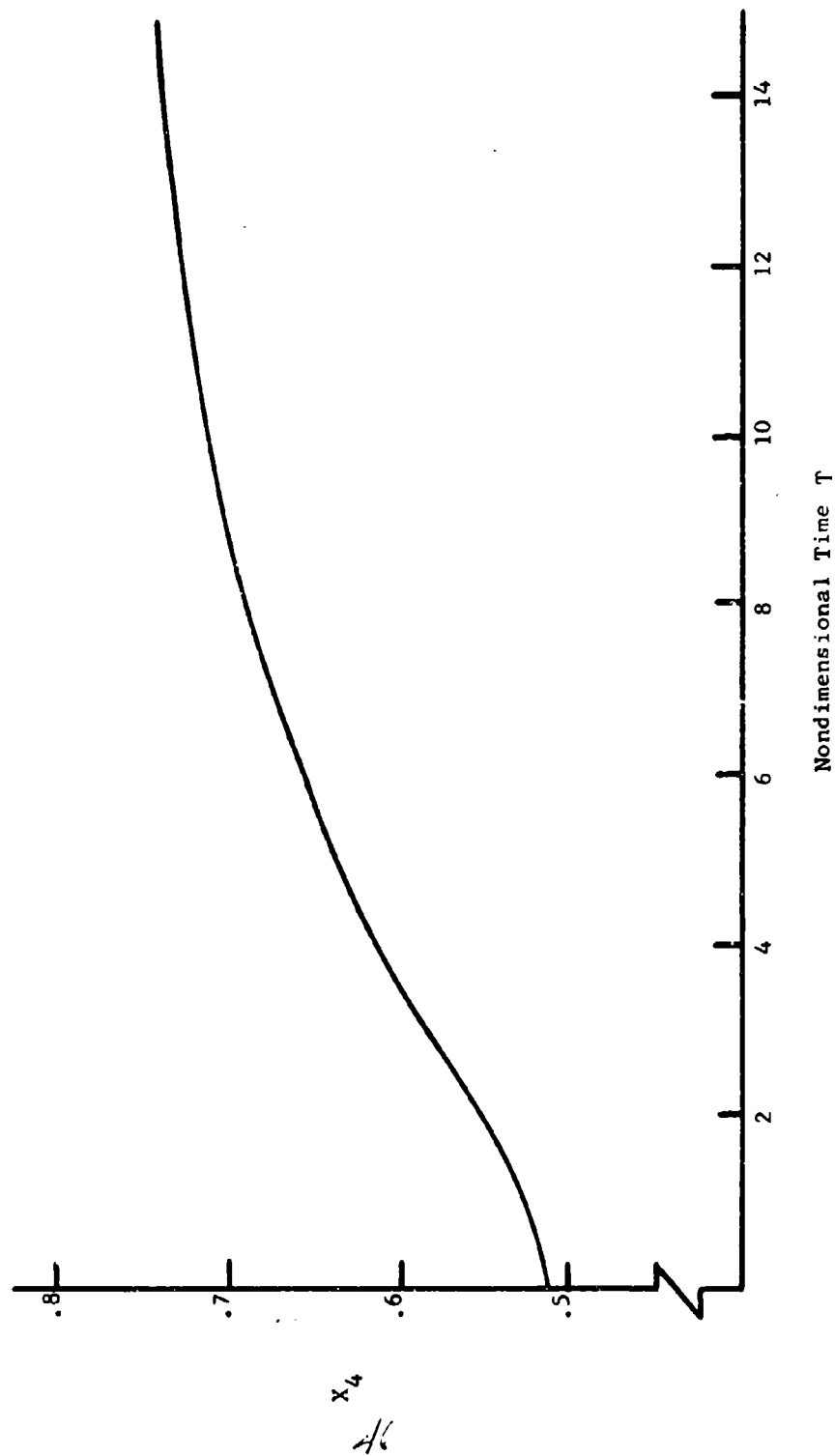


Figure 17. Dynamic Response of Bubble Mass ( $x_4$ ) for Case A.

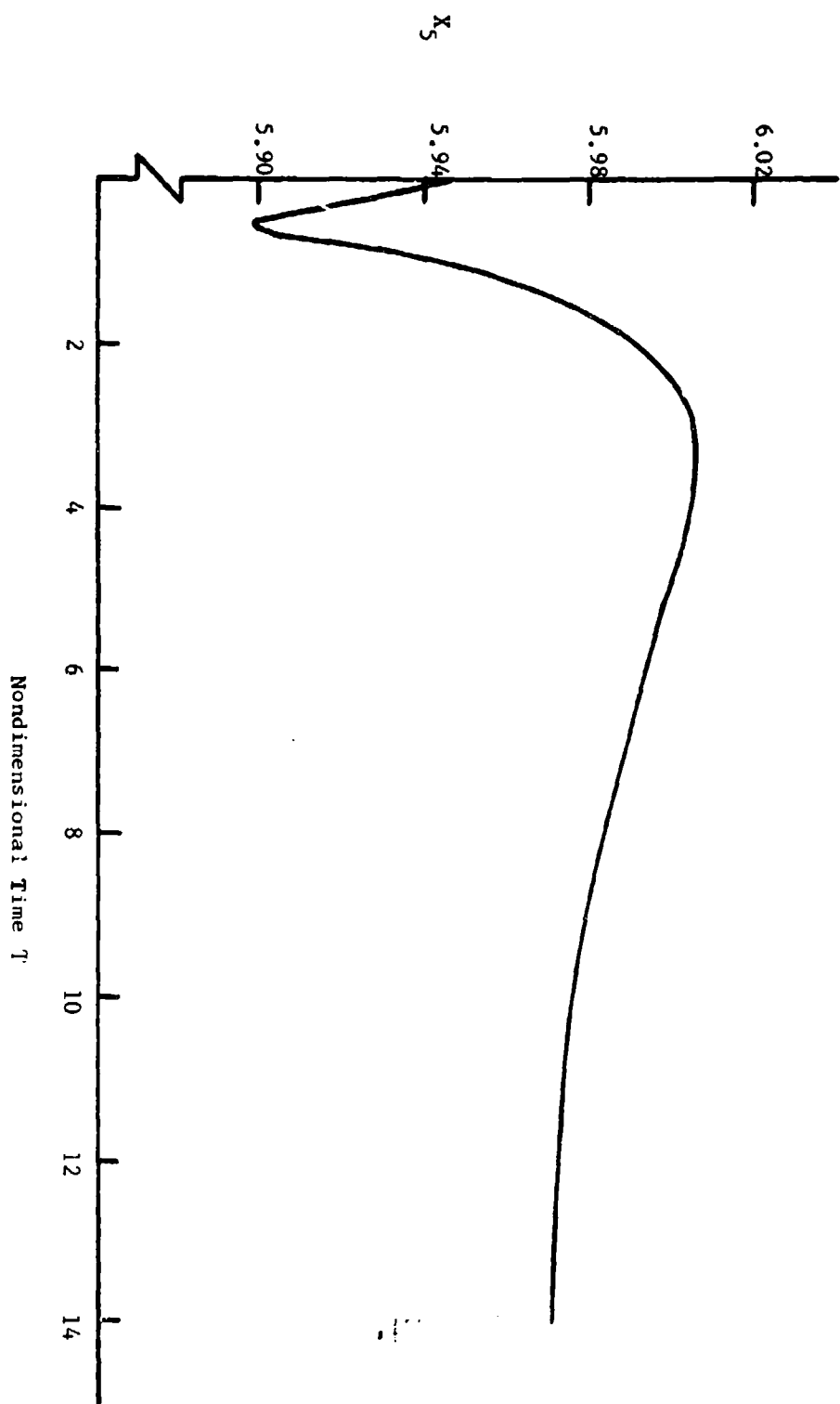


Figure 18. Dynamic Response of Bubble Pressure ( $X_s$ ) for Case A.

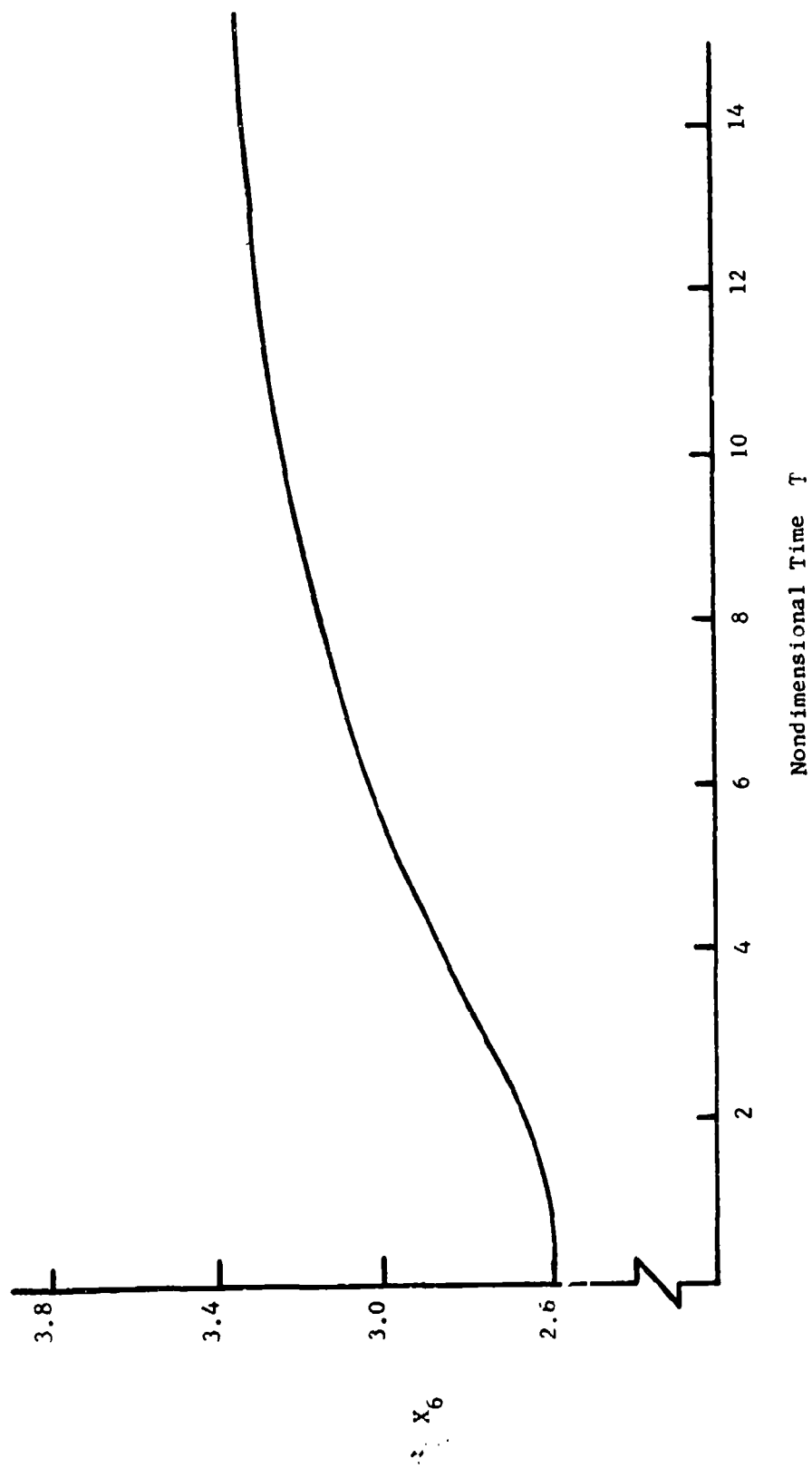


Figure 19. Dynamic Response of Reattachment Length ( $X_6$ ) for Case A.

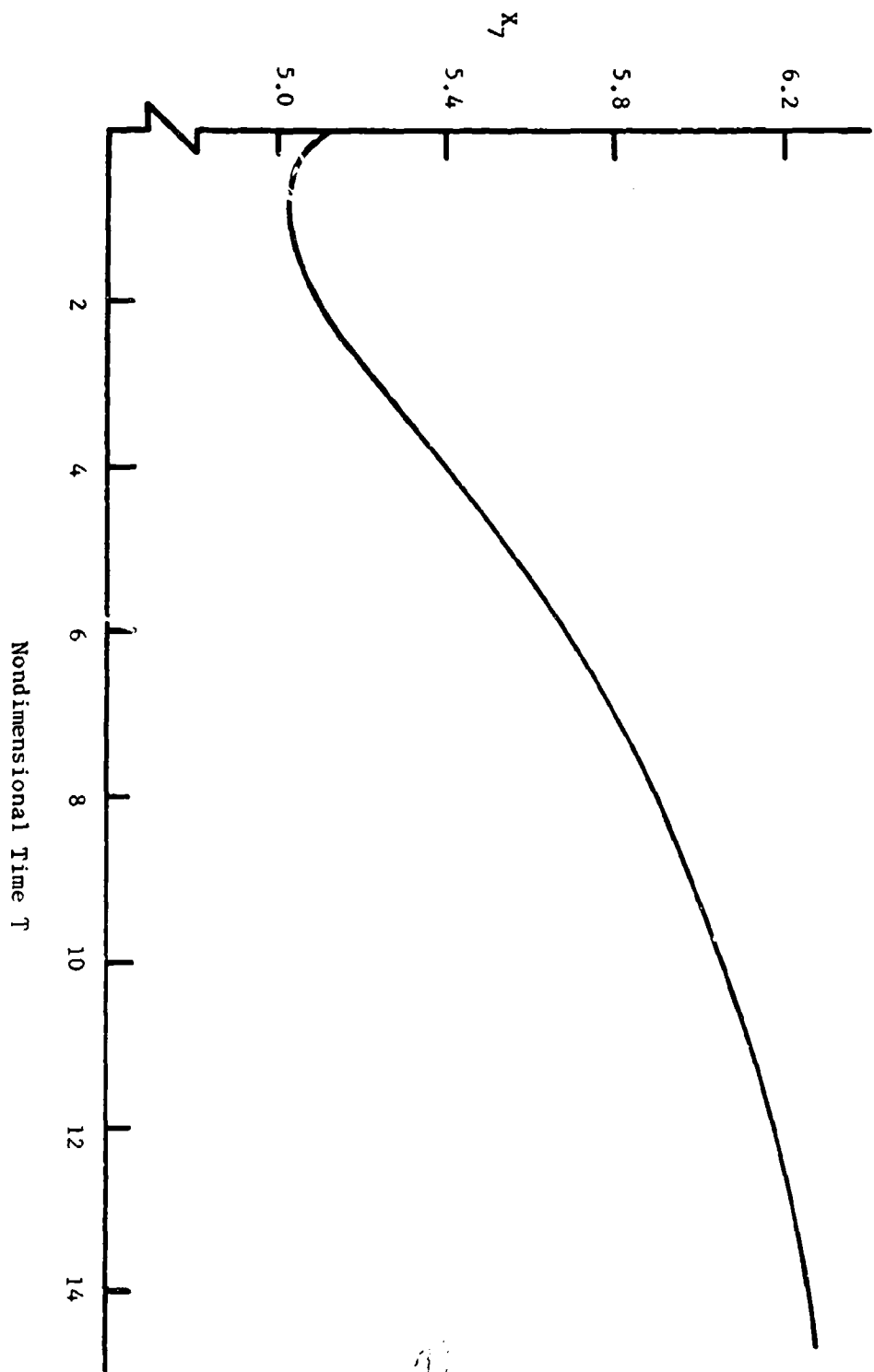


Figure 20. Dynamic Response of Jet Radius of Curvature ( $X_7$ ) for Case A.

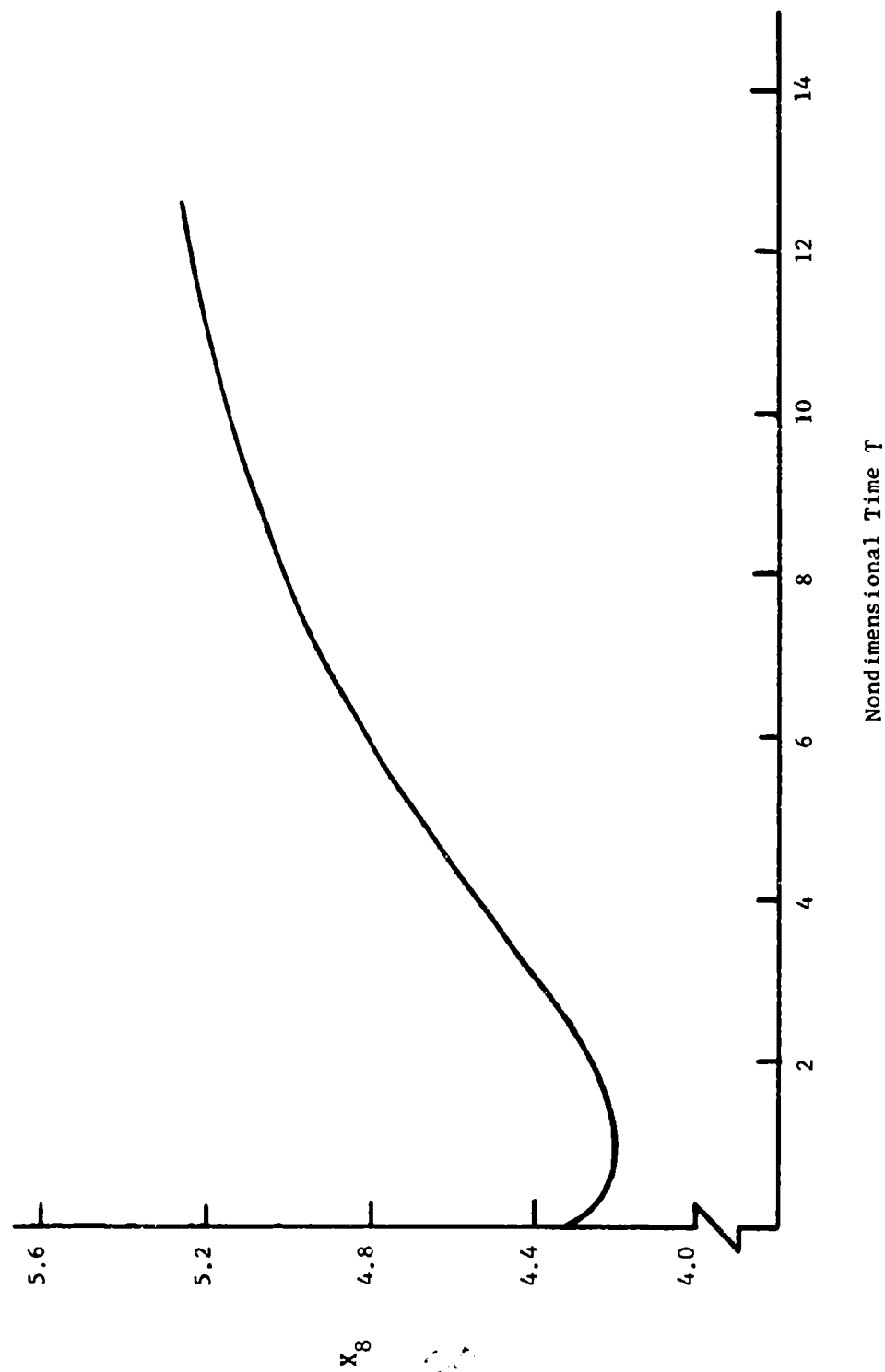


Figure 21. Dynamic Response of Reattachment Radius ( $X_8$ ) for Case A.

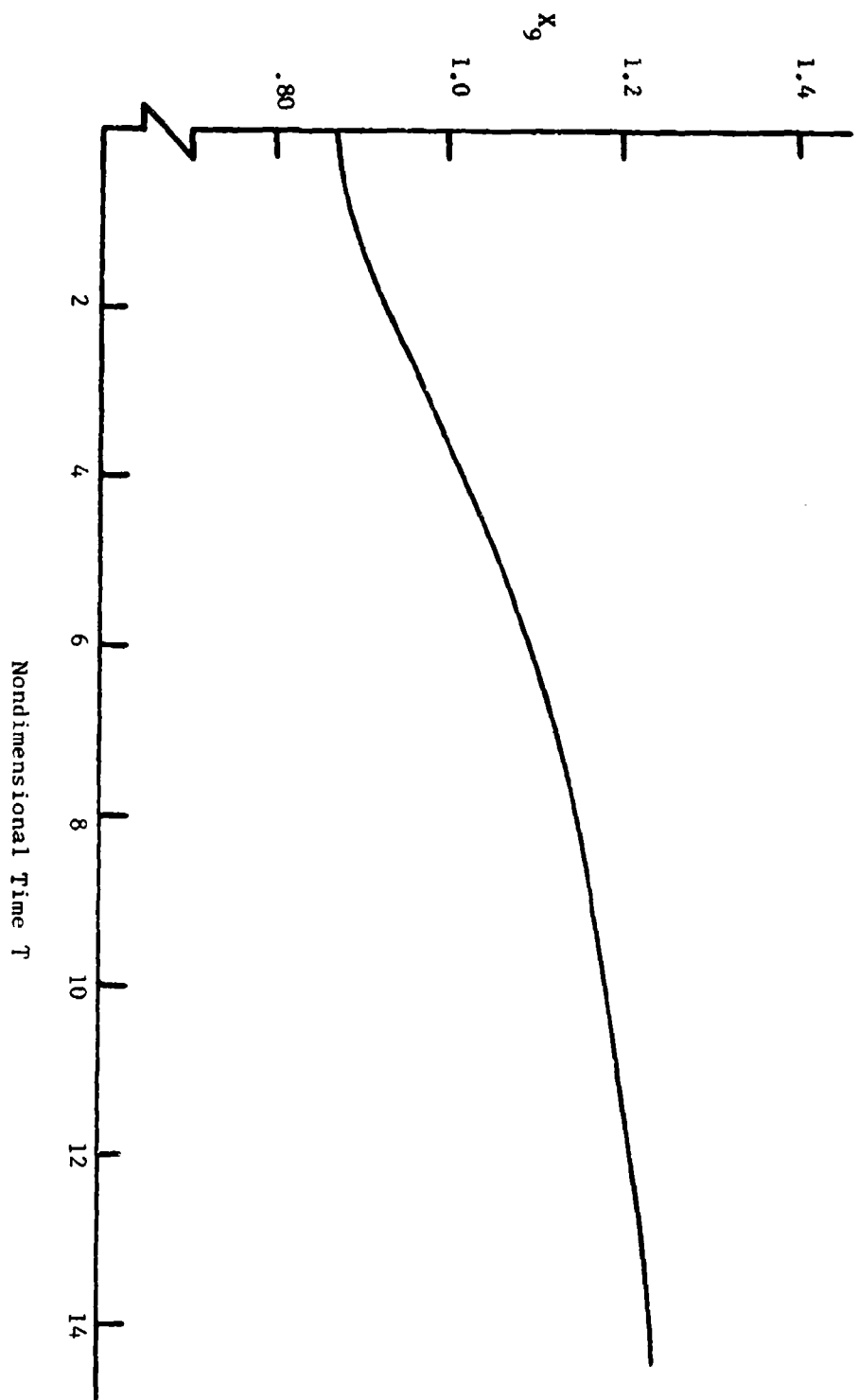


Figure 22. Dynamic Response of Bubble Volume ( $X_g$ ) for Case A.

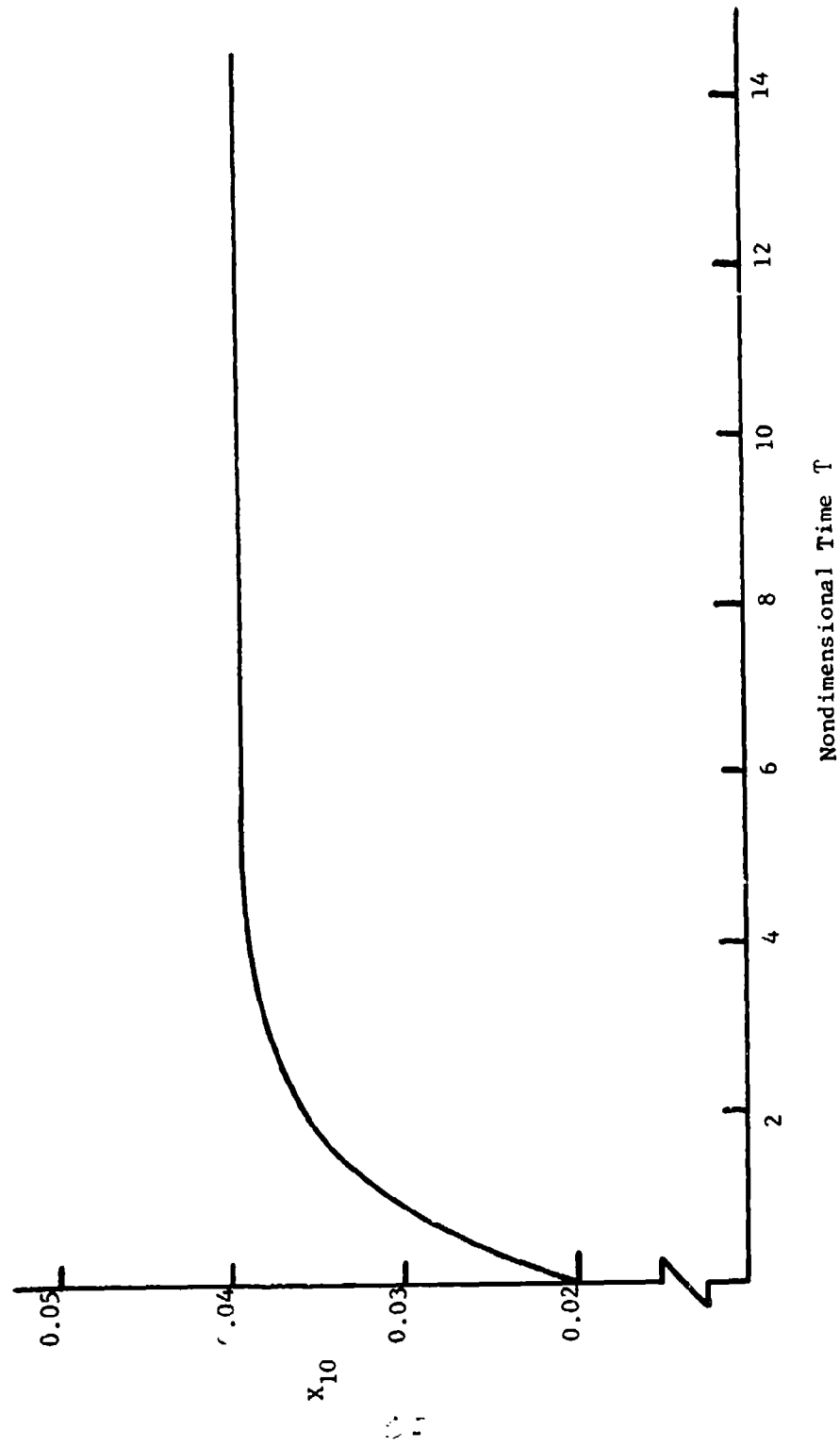


Figure 23. Dynamic Response of Angle  $\beta$  ( $X_{10}$ ) for Case A.

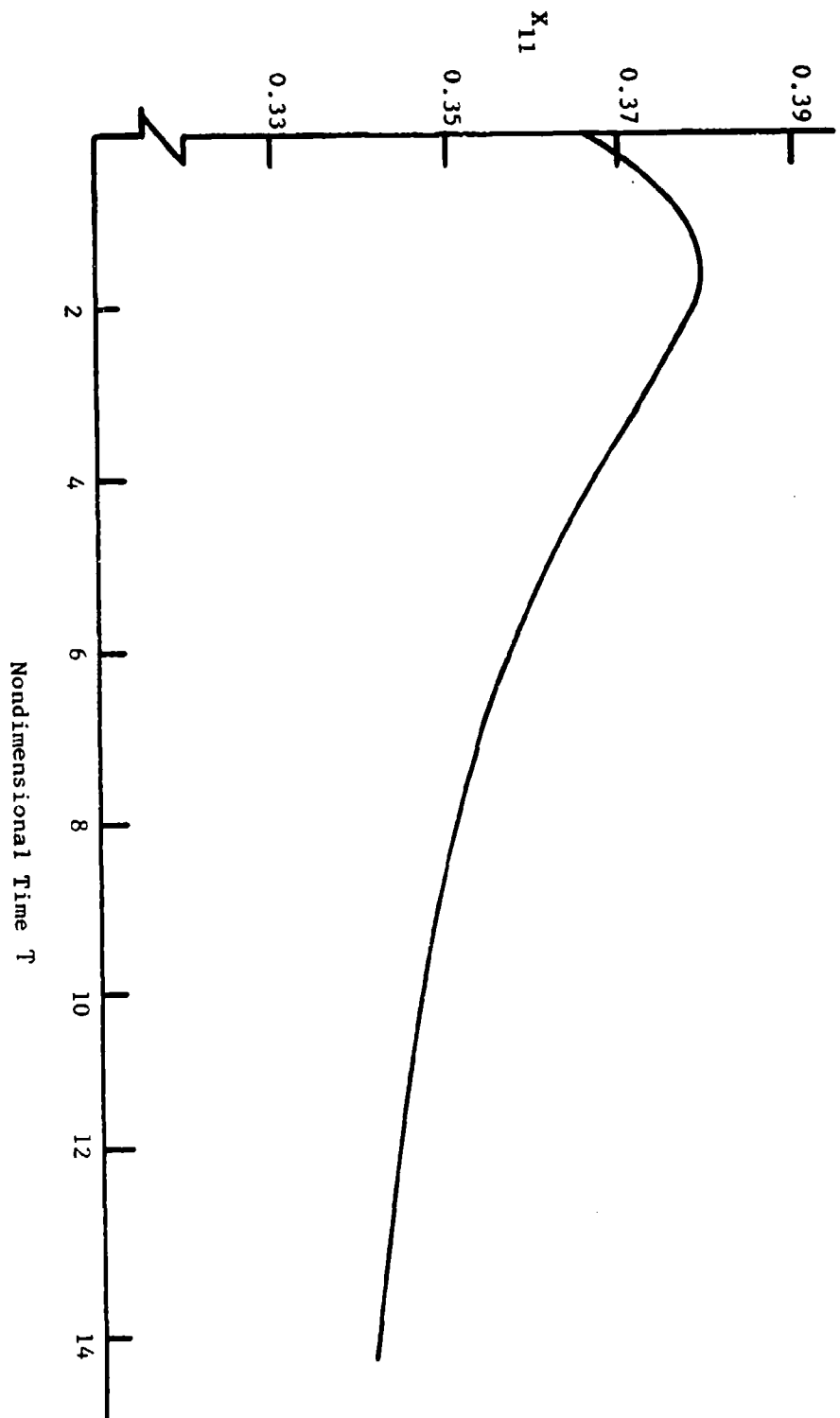


Figure 24. Dynamic Response of Angle  $\theta$  ( $X_{11}$ ) for Case A.



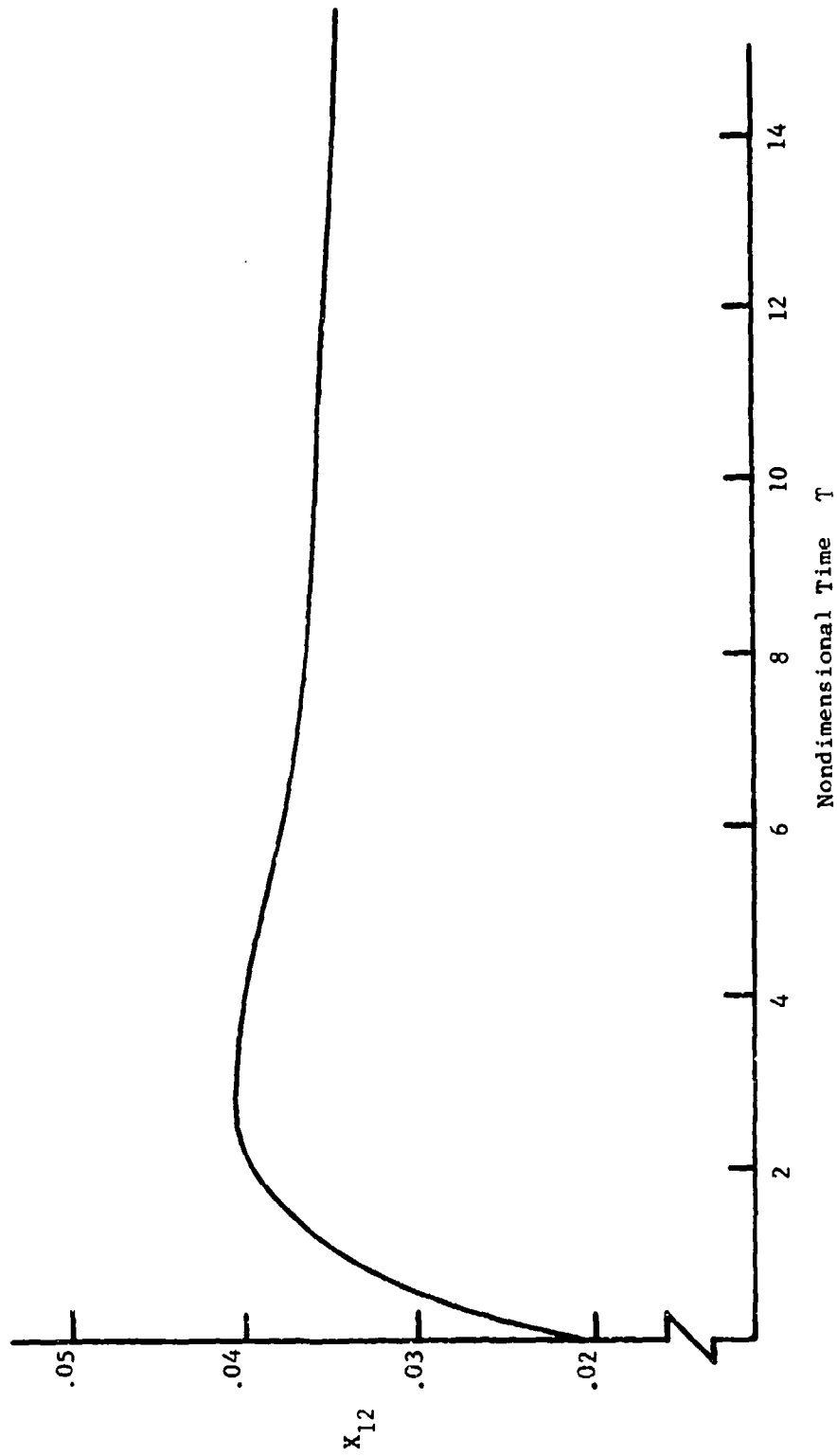


Figure 25. Dynamic Response of Angle  $\phi$  ( $X_{12}$ ) for Case A.

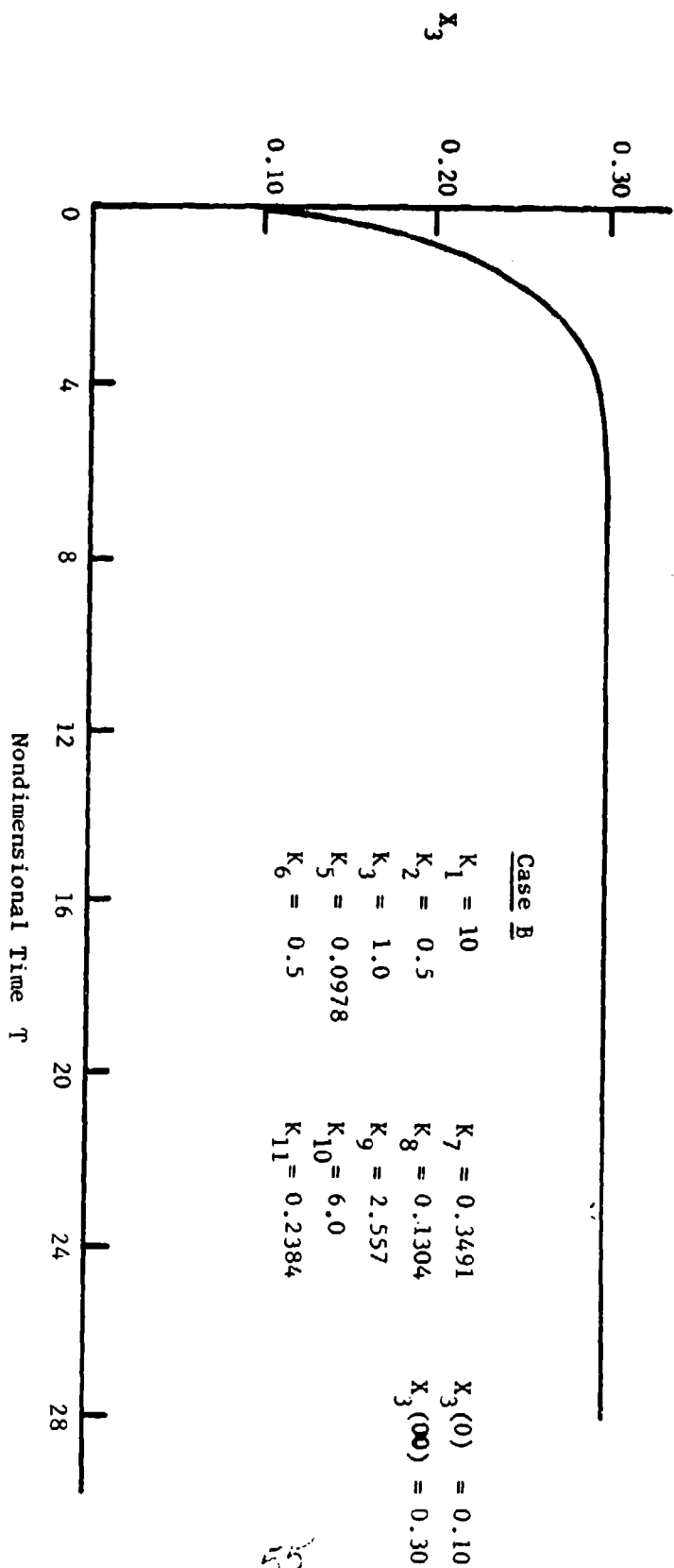


Figure 26. Dynamic Input for Case B - Large Change in Control Flow ( $X_3$ ).

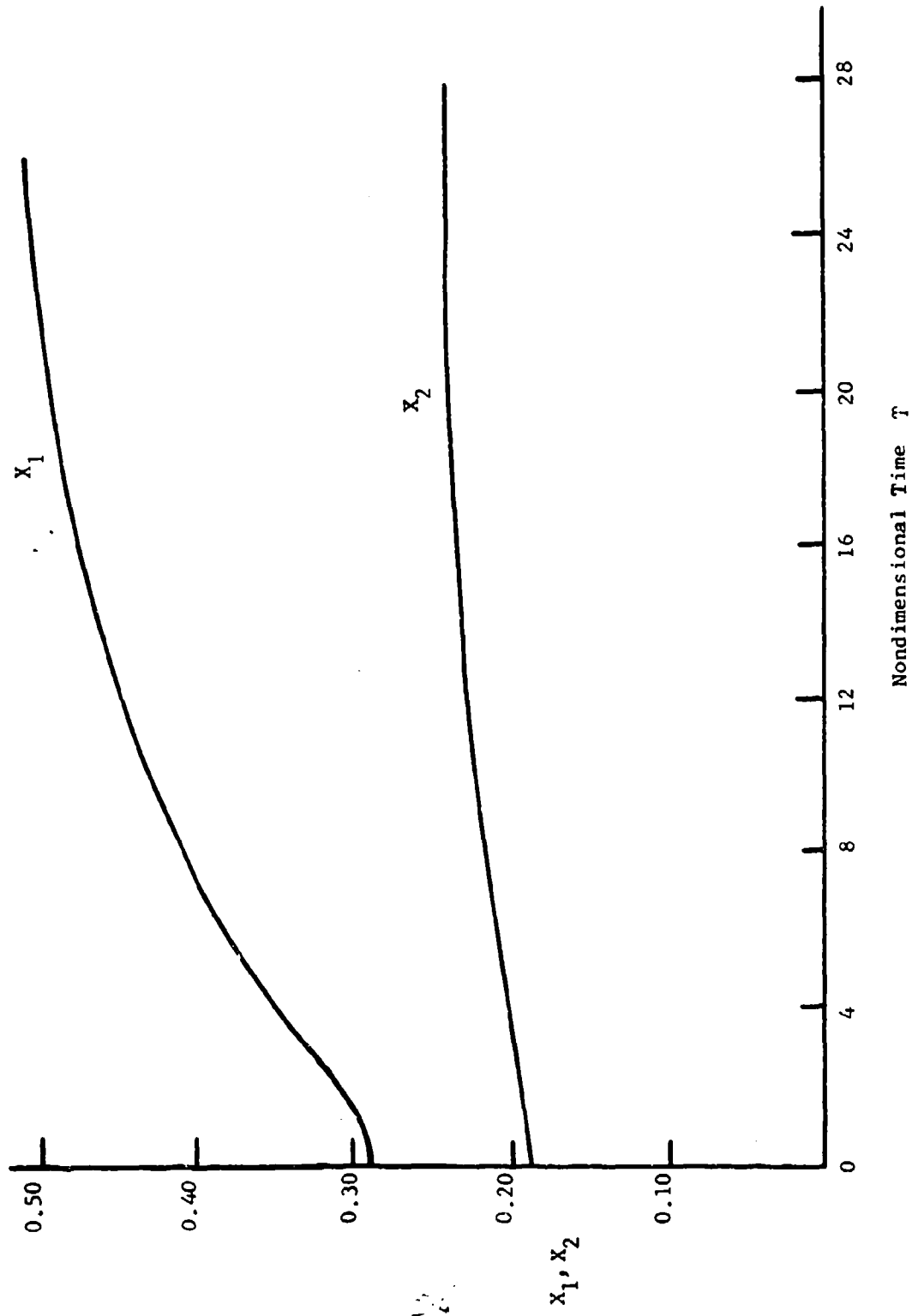


Figure 27. Dynamic Response of Entrainment and Recirculating Flows ( $X_1, X_2$ ) for Case B.

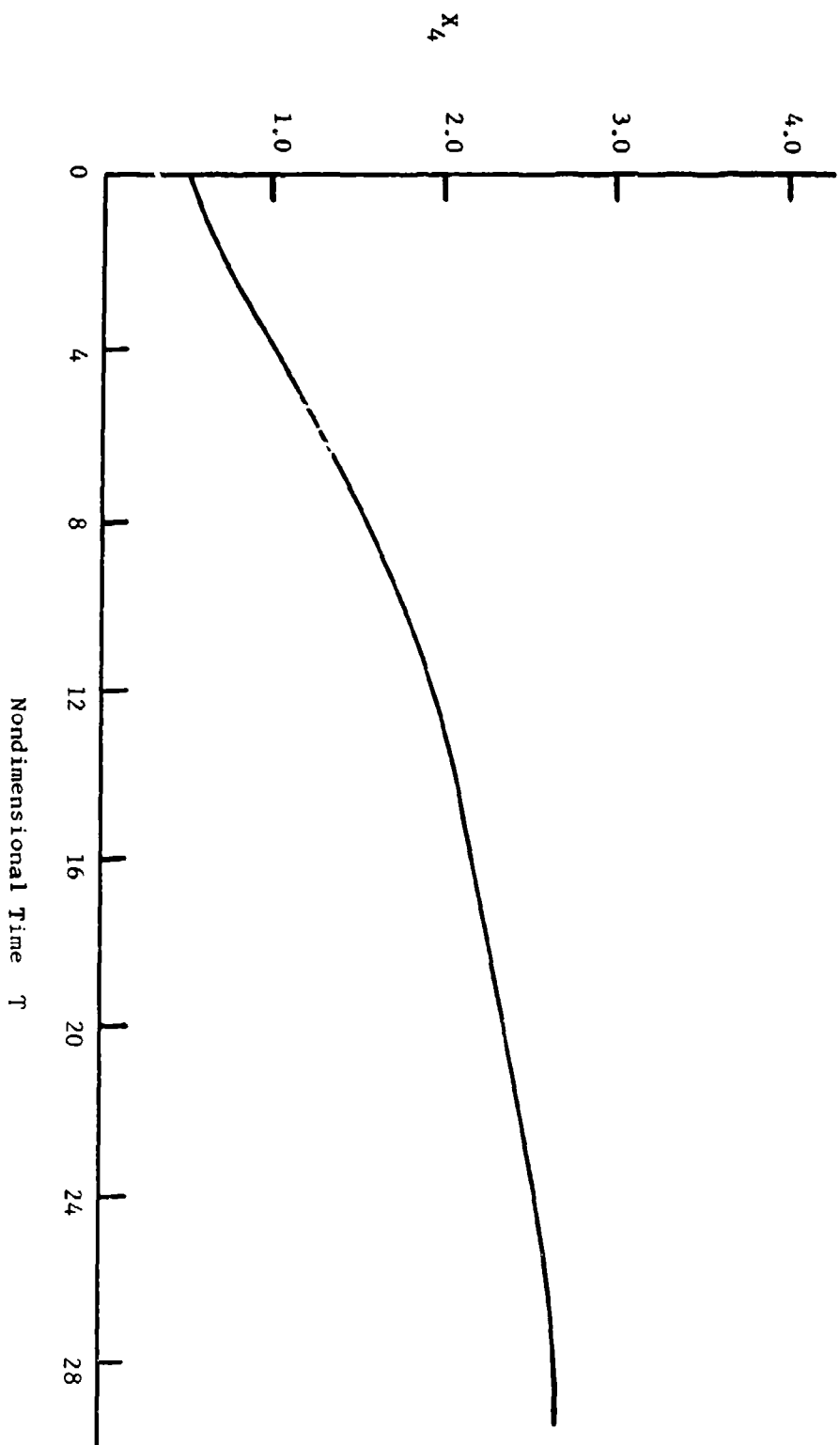


Figure 28. Dynamic Response of Bubble Mass ( $X_4$ ) for Case B.

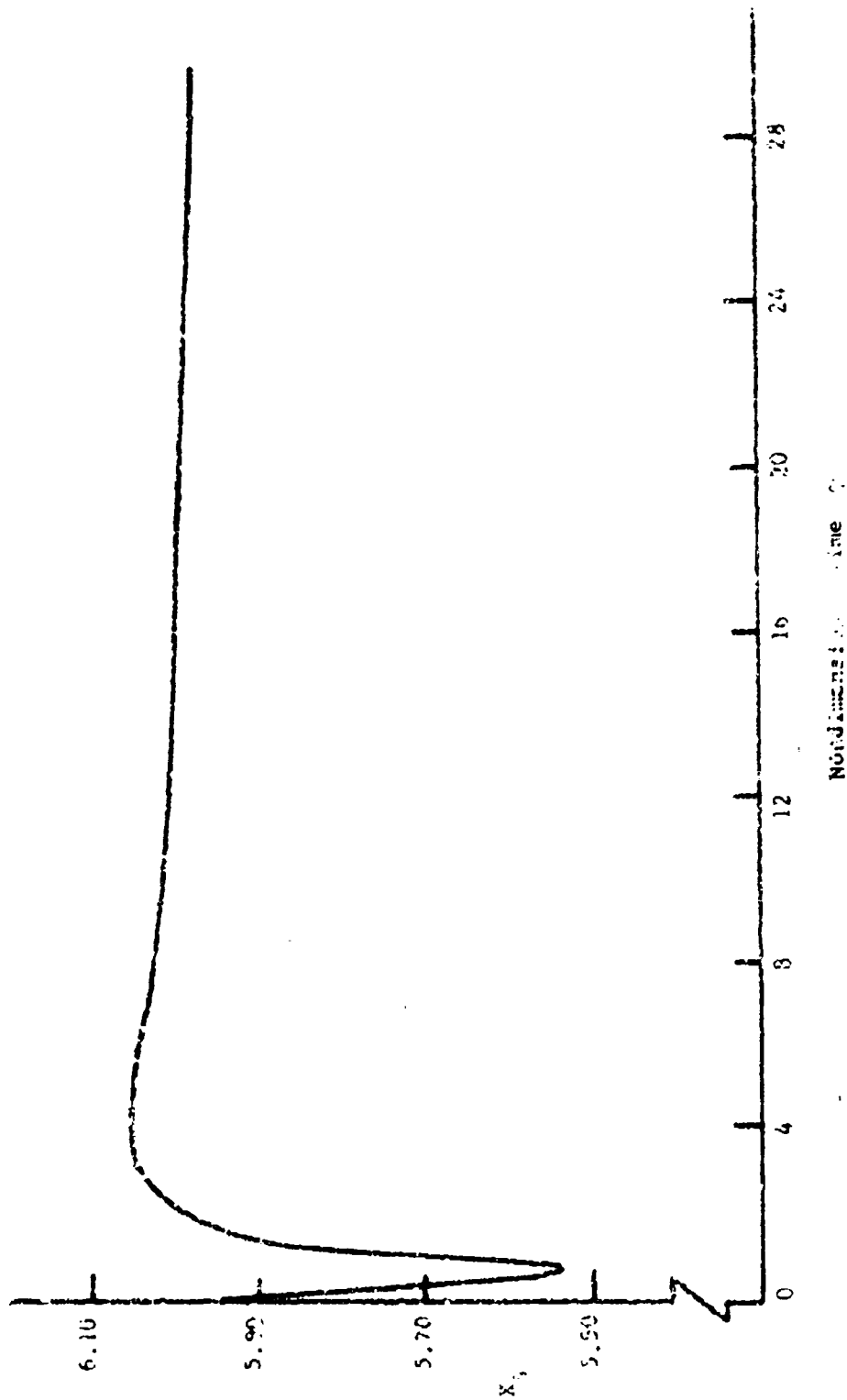


Figure 29. Dynamic Response of Bubble Pressure ( $X_5$ ) for Case B.

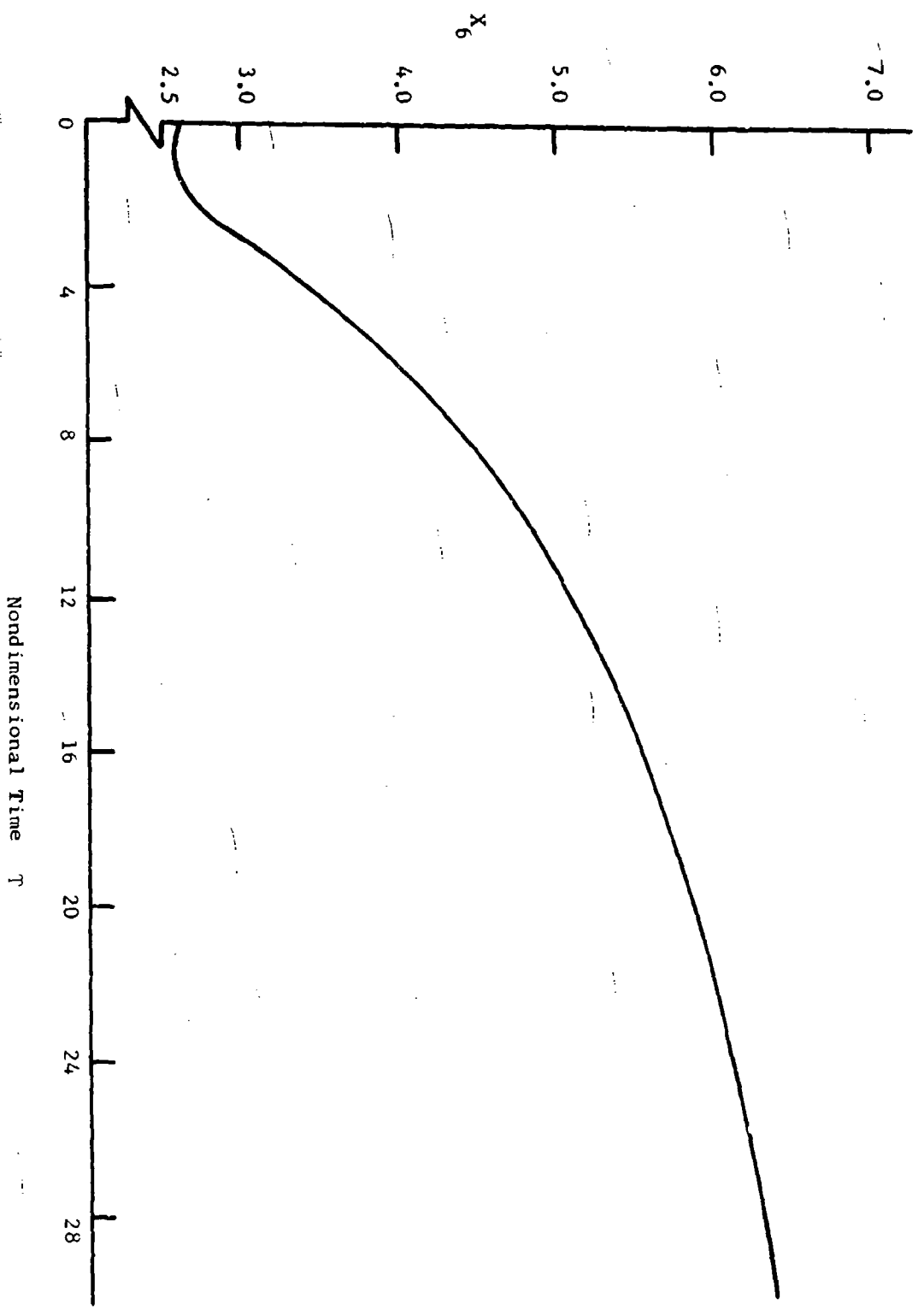


Figure 30. Dynamic Response of Reattachment Length ( $X_6$ ) for Case B.

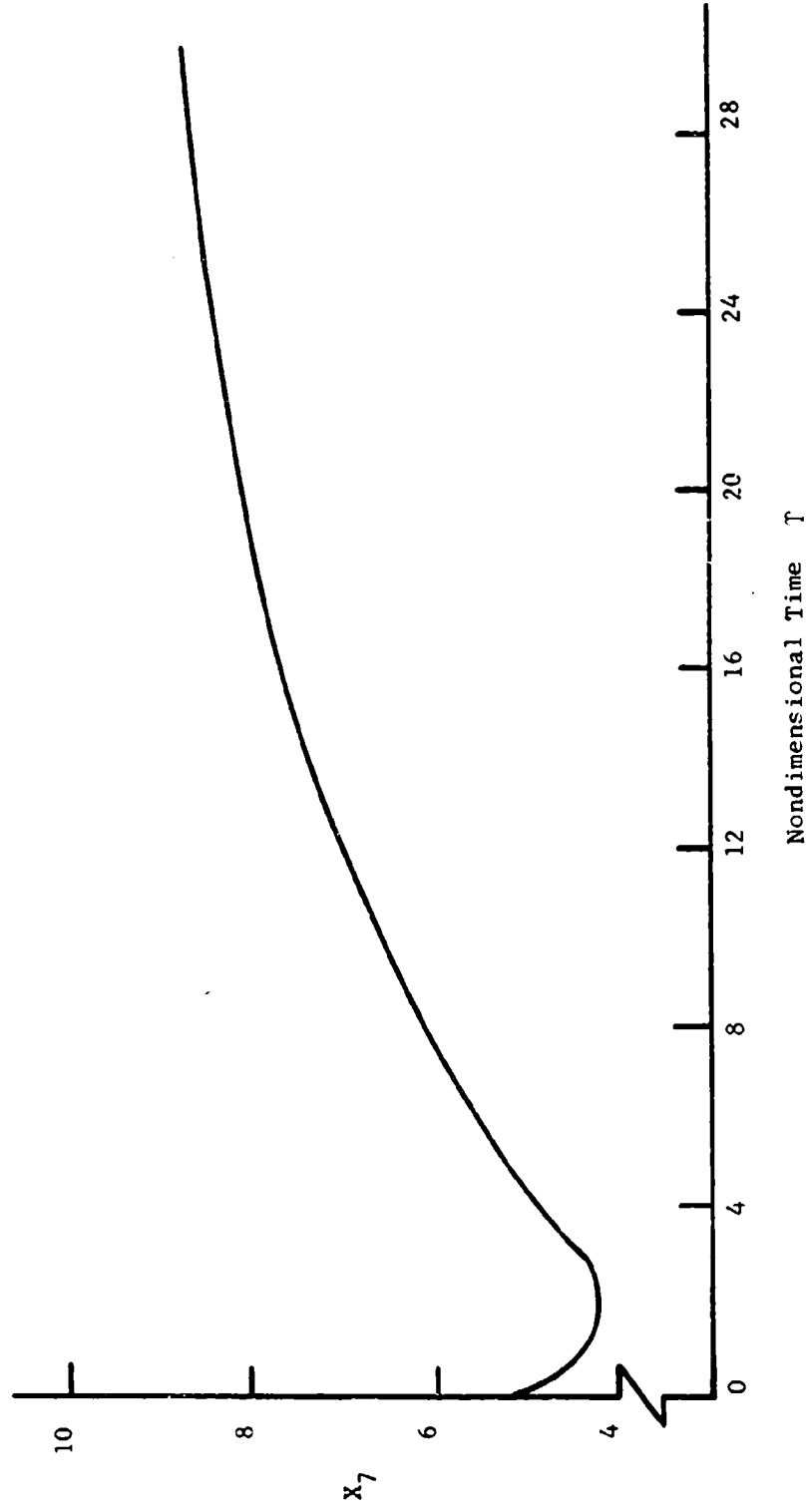


Figure 31. Dynamic Response of Jet Radius of Curvature ( $X_7$ ) for Case B.

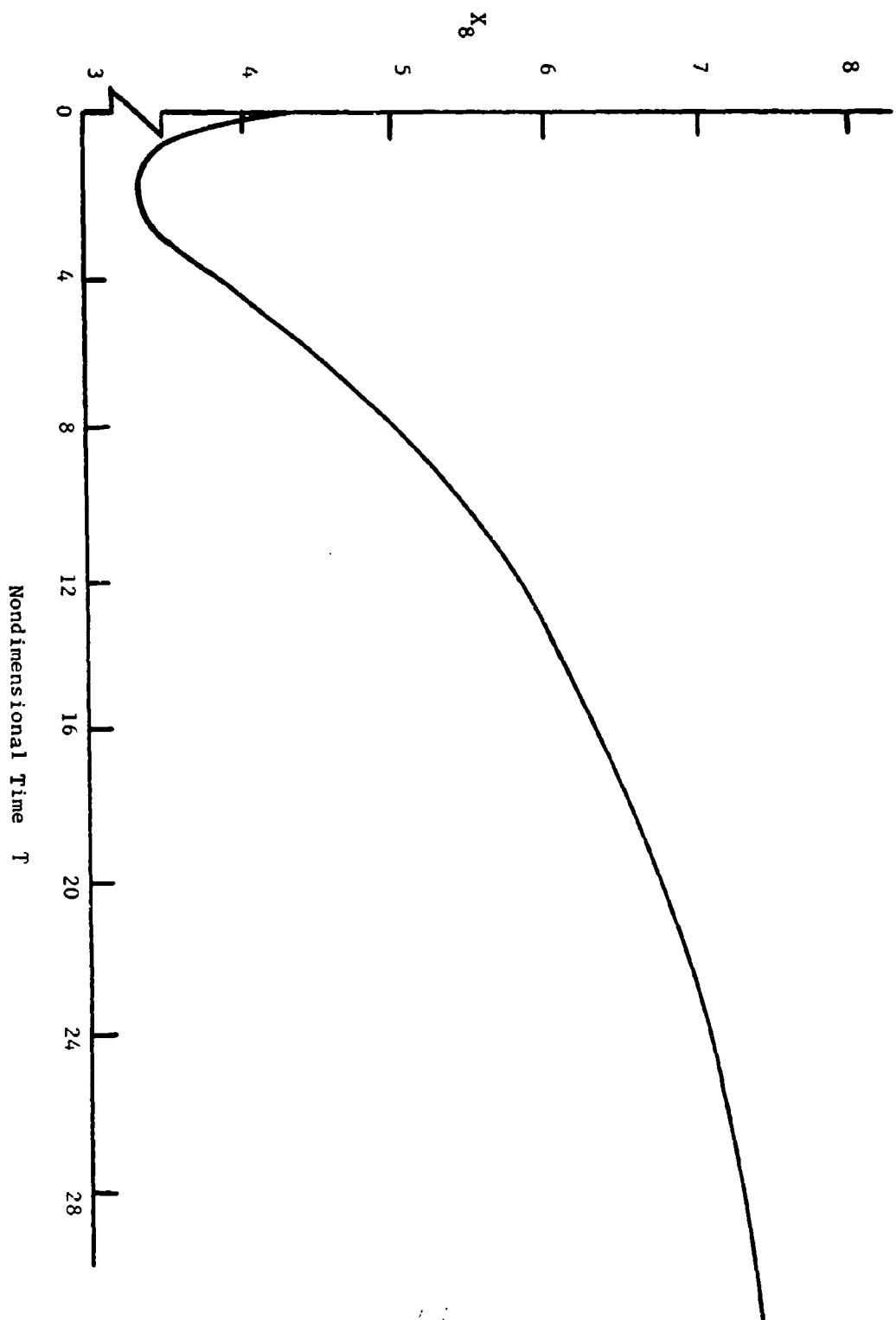


Figure 32. Dynamic Response of Reattachment Radius ( $X_g$ ) for Case B.



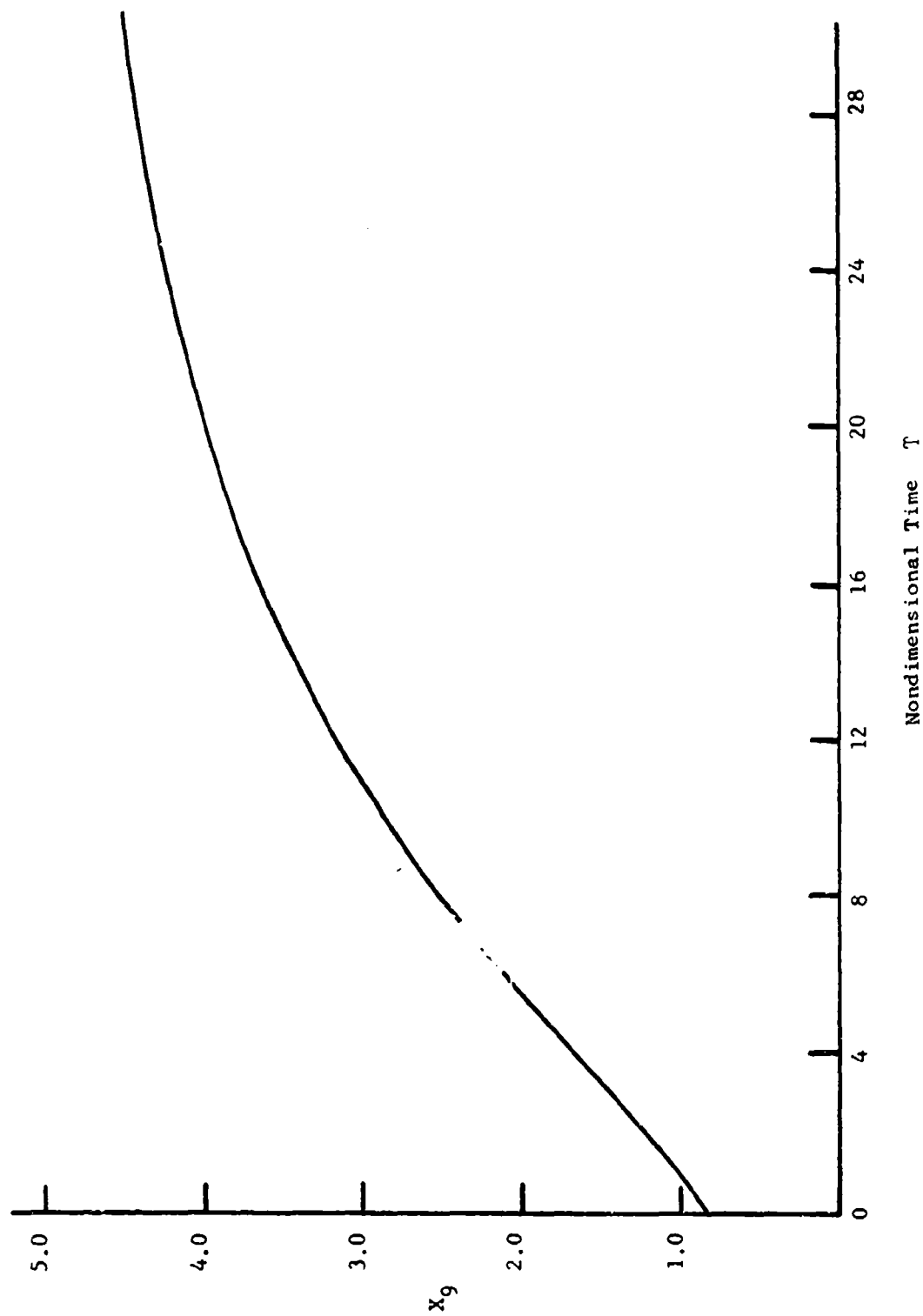


Figure 33. Dynamic Response of Bubble Volume ( $X_g$ ) for Case B.

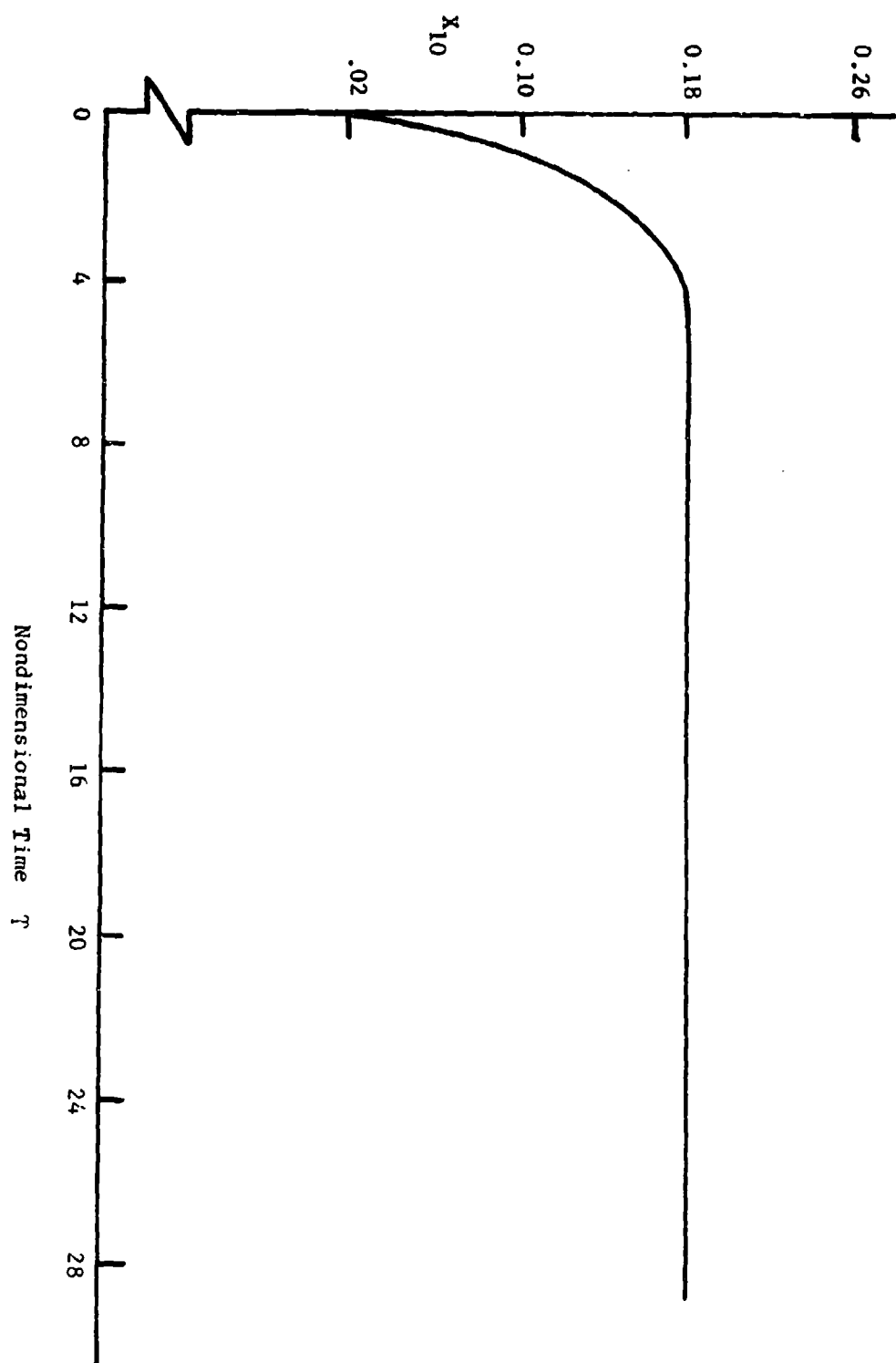


Figure 34. Dynamic Response of Angle  $\delta$  ( $X_{10}$ ) for Case B.

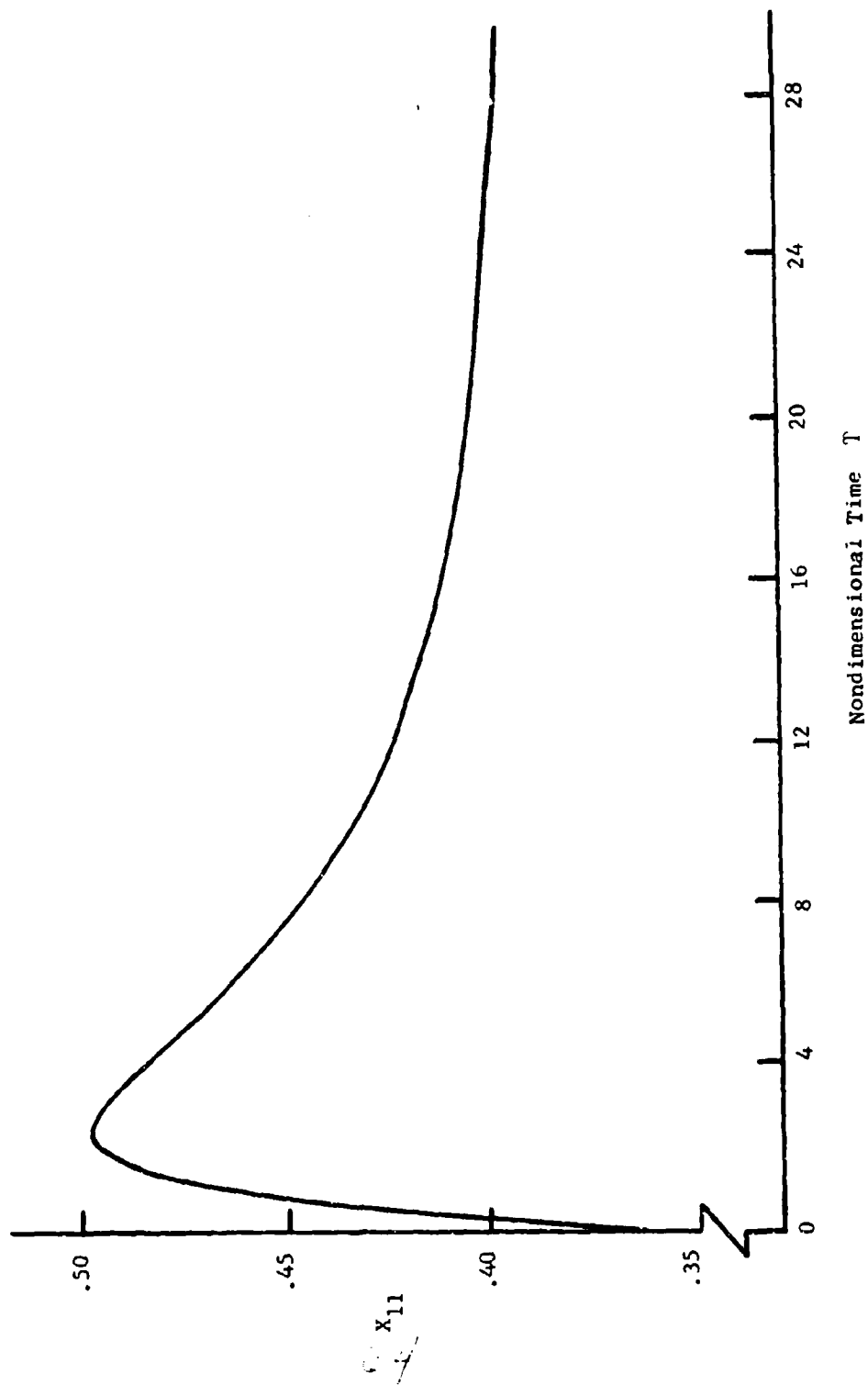


Figure 35. Dynamic Response of Angle  $\theta$  ( $X_{11}$ ) for Case B.

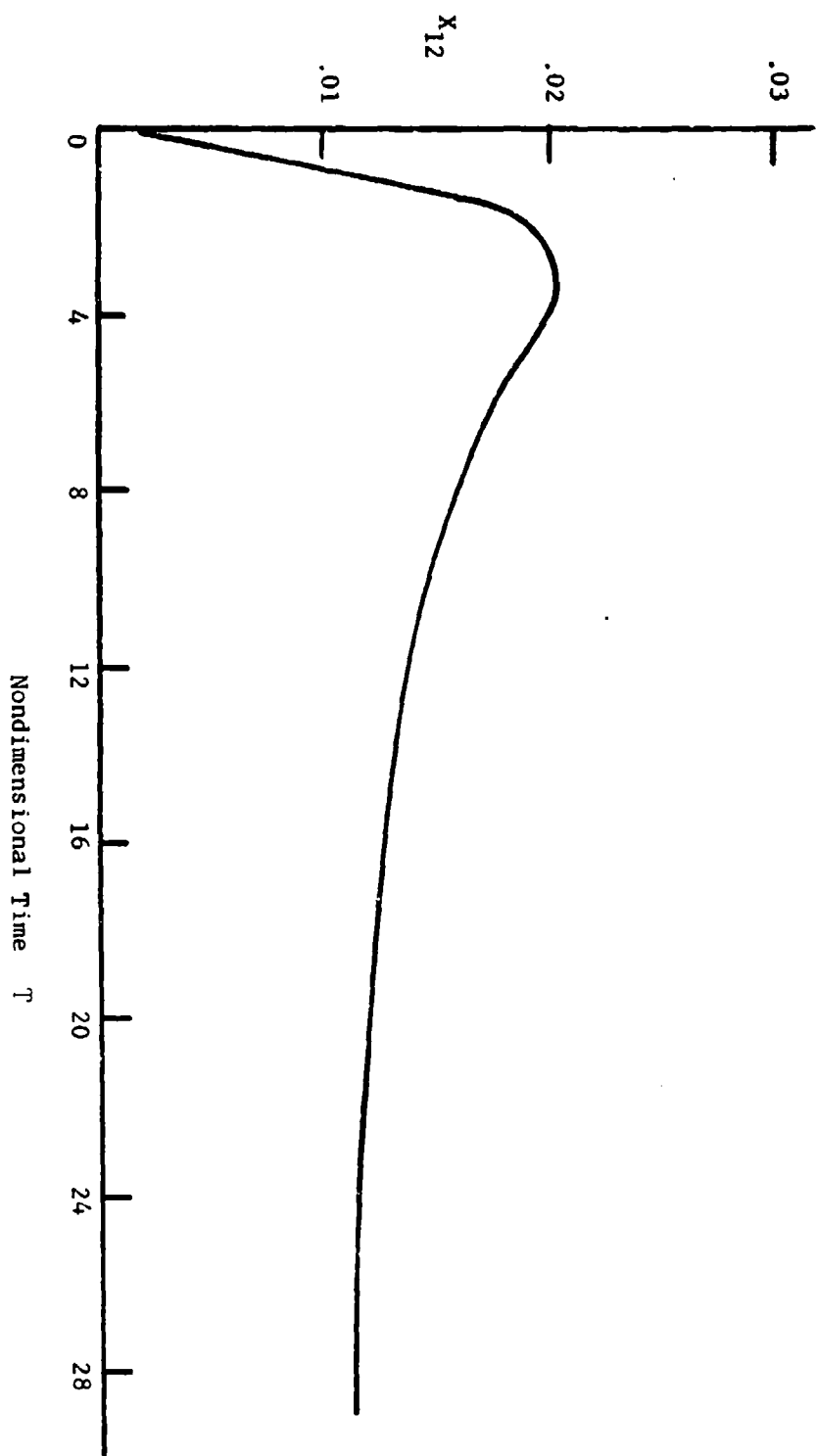


Figure 36. Dynamic Response of Angle  $\phi$  ( $X_{12}$ ) for Case B.